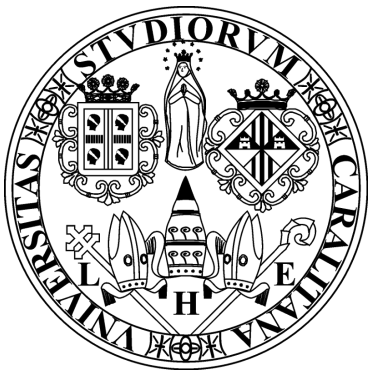


Università degli Studi di Cagliari

Facoltà di Scienze

Corso di Laurea Triennale in Fisica

Gravitational wave background from inflation: generation and detection

Relatori:

Prof. Delphine Perrodin

Candidato:

Ilaria Renoldi

matr. 60/60/65463

Anno Accademico 25/26

Contents

1 A BRIEF INTRODUCTION TO COSMOLOGY **1**

1.1 Aim and origin of modern cosmology 1

1.2 Geometry of the universe: the FLRW metric 3

1.3 Dynamics of the universe: the Friedmann Equations 5

1.4 Problems of the Big Bang model and introduction to inflation 9

2 A BRIEF INTRODUCTION TO GRAVITATIONAL WAVES **18**

2.1 Gravitational waves in General Relativity 18

2.2 Observational and physical properties of GWs 21

2.3 Gravitational Waves in FLRW background 24

3 COSMOLOGICAL PRODUCTION OF GRAVITATIONAL WAVES **28**

3.1 Introduction: the quantum nature of perturbations 28

3.2 Quantization of tensor modes and graviton production 30

3.3 Primordial Perturbations from single-field slow-roll inflation 32

3.3.1 The Bunch-Davies vacuum 32

3.3.2 Horizon exit and mode freezing 33

3.3.3 Power spectrum of primordial tensor modes 34

3.3.4 Tensor tilt 35

3.3.5 Scalar perturbations and consistency relation 35

3.4 Post-inflationary evolution and the stochastic background 36

3.4.1 Horizon re-entry and the quantum-to-classical transition 36

3.4.2 Evolution of tensor modes 37

3.4.3 The transfer function . . . 38
3.4.4 Present-Day energy density spectrum . . . 39
3.5 Beyond slow-roll: blue-tilted spectra from non-standard Scenarios . . . 39
3.5.1 Axion inflation and gauge field coupling . . . 40
3.5.2 Spectator fields with low sound speed . . . 40
3.5.3 Effective Field Theory (EFT) and Modified Gravity . . . 41
3.5.4 Post-inflationary enhancement: the stiff era . . . 41
3.6 Beyond linear order: scalar induced gravitational waves . . . 42
3.6.1 Second-order Einstein equations and the source term . . . 42
3.6.2 Power spectrum and features . . . 43
3.6.3 Alternative cosmological mechanisms of GW production . . . 44

4 OBSERVATIONAL PERSPECTIVES ON STOCHASTIC GRAVITATIONAL-WAVE BACKGROUNDS 46

4.1 Gravitational wave detection . . . 47
4.1.1 Interferometric principle . . . 47
4.1.2 Gravitational wave detectors . . . 48
4.2 Constraints on inflation models from the CMB . . . 50
4.3 Background detection: recent results and implications . . . 53

CONCLUSIONS 57

Abstract

The advent of gravitational-wave astronomy, inaugurated by the first direct detection by the Laser Interferometer Gravitational-Wave Observatory (LIGO) in 2015, has opened an unprecedented observational window onto the Universe. While current detections primarily probe astrophysical systems, gravitational waves also represent the only messenger capable of carrying direct information from the earliest moments of cosmic history — epochs inaccessible to electromagnetic observations, including those of the Cosmic Microwave Background (CMB). In particular, a stochastic background of primordial origin would provide access to energy scales far beyond those achievable in terrestrial experiments.

This thesis aims to explore the physics of primordial gravitational waves (PGWs), investigating their production, evolution, and observational implications within the framework of single-field slow-roll inflation. Tensor perturbations are treated as quantum fluctuations of the metric evolving in a quasi–de Sitter spacetime. Their amplification during inflation leads to a nearly scale-invariant primordial tensor power spectrum, whose amplitude depends on the Hubble parameter during inflation. The tensor spectral tilt and the tensor-to-scalar ratio are discussed as key observables which encode information about the inflationary energy scale and the dynamics of the inflaton field.

The subsequent evolution of tensor modes is examined by following their horizon re-entry during the radiation- and matter-dominated eras. The transfer function formalism is introduced to connect the primordial spectrum to present-day observables, allowing for the computation of the spectral energy density of the stochastic gravitational-wave background today. In the minimal inflationary scenario, the resulting spectrum is slightly red-tilted and predicts an amplitude well below the sensitivity of current interferometric detectors, although it is fully consistent with the stringent bounds derived from CMB observations, particularly from the absence of primordial B-mode polarization.

Motivated by this observational limitation, the thesis discusses extensions beyond the minimal scenario that can enhance the gravitational-wave signal. These include mechanisms capable of producing blue-tilted spectra or localized features, scalar-induced gravitational waves

generated at second order in perturbation theory, and particle production effects due to couplings between the inflaton and additional fields. The possible contribution of other early-Universe sources, such as first-order phase transitions and cosmic strings, is also briefly addressed.

Finally, theoretical predictions are confronted with the current observational landscape. The complementarity between CMB constraints at large scales and direct searches performed by ground-based interferometers, space-based missions, and Pulsar Timing Arrays (PTAs) is emphasized. Particular attention is devoted to the 2023 PTA results reporting evidence for a common-spectrum stochastic signal at nanohertz frequencies. While this signal is most plausibly interpreted as astrophysical in origin, its characterization provides important guidance for inflationary and alternative cosmological models.

Overall, this work highlights how the interplay between quantum field theory in curved spacetime, early-Universe cosmology, and multi-band gravitational-wave observations can progressively constrain models of inflation and high-energy physics, bringing us closer to a direct experimental window onto the physics of the primordial Universe.

Chapter 1

A BRIEF INTRODUCTION TO COSMOLOGY

1.1 Aim and origin of modern cosmology

Since the dawn of civilization, the sky has been a source of interest and investigation for humankind. Ancient cultures first attempted to fathom the cosmos through myths, such as the flat-Earth model of the Egyptians. Centuries later, using observation and geometrical intuition, Greek philosophers imagined a cosmological model with the earth in the center and fixed stars in an outer celestial sphere; within this framework, they were able to deduce the sizes and distances of the Earth, Moon, and Sun with remarkable accuracy for their time. Over the centuries, these efforts evolved into the first geometrical and mathematical descriptions of the firmament, culminating in the heliocentric model proposed by Copernicus in the sixteenth century. His motivation was not direct observation, but the mathematical simplicity offered by placing the Sun at the center: a first step from philosophy toward a quantitative physical model of the solar system [1].

Yet, cosmology differs from most branches of physics, since it studies a single object: our Universe. The data available to test cosmological models come from a finite observable region, tied to our specific position in spacetime. For this reason, cosmological theories cannot be falsified in the same way as laboratory experiments; their validity is assessed through consistency between theoretical predictions and astronomical observations: it is therefore important

to distinguish between the observable Universe, which we can study and measure, and the Universe as a whole, which may include regions forever beyond our causal reach [2].

A decisive turning point came in the early twentieth century with Einstein's theory of General Relativity (1915). Although not conceived as a cosmological theory, it provided the conceptual framework on which modern cosmology is built. Despite the initial skepticism it met (due to its mathematical complexity and counter-intuitive predictions), General Relativity soon found solid confirmation in observations, such as the precession of Mercury's perihelion, the deflection of starlight by the Sun observed in 1919, and the gravitational redshift measured in 1925. A century later, the first detection of gravitational waves (2015) provided one of its most striking experimental validations [3].

Only with the development of General Relativity did cosmology acquire a less speculative character, entering an era of precision. By solving Einstein's equations, which allowed for a mathematical description of spacetime as a dynamic system, Friedmann and Lemaître demonstrated that the Universe could be expanding [2].

Years earlier, in the 1910s, Vesto Slipher measured the displacement of spectral lines in the light from distant galaxies. He interpreted this shift as a Doppler effect, implying that many galaxies were moving away from us. Within the relativistic framework established by Einstein and Friedmann, about a decade later, Georges Lemaître reinterpreted Slipher's data, correctly proposing that the observed redshift did not arise from the motion of galaxies through space, but from the expansion of space itself. This marked the first quantitative link between General Relativity and cosmological observations.

The hypothesis was soon reinforced by the work of Edwin Hubble, who in 1929 established a clear empirical correlation between the redshift of distant galaxies and their distances. His data revealed a linear relation, now known as the Hubble–Lemaître law, expressed as

$$z \approx \frac{H_0}{c} r \qquad \text{with } z \ll 1 \tag{1.1}$$

where z is the cosmological redshift, H_0 the present-day Hubble parameter, c the speed of light and r the distance to the source

showing that further galaxies exhibit proportionally higher redshifts. This observation proved that the Universe is expanding uniformly in all directions.

The expansion can be described by a single time-dependent quantity, the scale factor a(t), which characterizes how distances between comoving points change over cosmic time. The rate of this expansion is quantified by the Hubble parameter

$$H(t) = \frac{\dot{a}(t)}{a(t)} \tag{1.2}$$

whose present value , $H_0 = H(t_0)$, corresponds to the slope measured in the original Hubble relation. The Hubble parameter provides a direct link between observation and theory: for small redshifts, the linear relation $v \approx H(t_0)d$ connects the recession velocity of galaxies to their proper distance [1].

Based on these results, cosmologists reconstructed the history of an expanding cosmos. The study of the physics of a stretching spacetime led, in the 1950s and 1960s, to the formulation of the hot Big Bang model, which became the prevailing paradigm after the detection of the Cosmic Microwave Background in 1965. From that moment, cosmology has been firmly grounded in observation and in the framework of General Relativity, establishing itself as a mature physical science, capable of connecting the physics of the smallest scales with the evolution of the largest structures in the Universe.

1.2 Geometry of the universe: the FLRW metric

Astronomical observations show that, when viewed on sufficiently large scales, the distribution of galaxies appears to be roughly uniform in every direction. This motivates the *cosmological principle*, the assumption that the Universe is homogeneous and isotropic on large scales (beyond $\sim$ 100 Mpc). This principle is a modern extension of the Copernican idea that no spatial location is privileged [2].

In special relativity, the separation between two events in flat spacetime is described by the invariant interval

$$ds^2 = -c^2dt^2 + dr^2 + r^2d\Omega^2 = -c^2dt^2 + \delta_{ij}\, dx^i dx^j, \tag{1.3}$$

corresponding to the Minkowski metric

$$\eta_{\mu\nu} = \mathrm{diag}(-1, 1, 1, 1). \tag{1.4}$$

This metric represents a static, flat spacetime and contains no effects of gravity [4].

When one assumes that the Universe looks the same at every point and in every direction, the spatial curvature must be constant across each spatial slice. Under this condition, only three types of spatial geometries are possible: positively curved (spherical), flat (Euclidean), or negatively curved (hyperbolic).

A spacetime metric that incorporates these three possibilities, and at the same time allows for a global expansion that may vary with time, is the Friedmann-Lemaître-Robertson-Walker (FLRW) metric:

$$ds^2 = -c^2dt^2 + a^2(t)\left[\frac{dr^2}{1-kr^2/R_0^2} + r^2 d\Omega^2\right], \tag{1.5}$$

where $a(t)$ is the scale factor, $k = \{+1, 0, -1\}$ labels closed, flat, and open geometries, R_0 is a curvature radius setting the spatial length scale, and $d\Omega^2 = d\theta^2 + \sin^2\theta\, d\phi^2$ denotes the line element on a sphere of radius 1, i.e. the angular part of the metric expressed in spherical coordinates [2].

The radial coordinate r is the *comoving coordinate*: it labels positions that remain fixed with respect to the cosmic expansion. The physical (proper) distance at time t between two comoving points in flat coordinates ($k = 0$) is therefore

$$d_{\rm phys}(t) = a(t)\, r, \tag{1.6}$$

showing that comoving separations stay constant while proper distances grow in proportion to $a(t)$.

The cosmic proper time t is the time measured by observers moving with the Hubble flow. For many applications, in particular those involving light propagation, it is convenient to introduce the conformal time

$$\tau(t) = \int_0^t \frac{dt'}{a(t')}, \tag{1.7}$$

in terms of which the metric in flat spatial coordinates takes the form

$$ds^2 = a^2(\tau)\left(-d\tau^2 + d\chi^2 + \chi^2 d\Omega^2\right). \tag{1.8}$$

The conformal time factors out the expansion of the Universe, so that light rays satisfy $d\chi = \pm d\tau$, following straight-line trajectories as they would in Minkowski spacetime.

The FLRW metric depends only on the function $a(t)$, which determines the entire expansion history. It also exhibits a rescaling symmetry: the overall normalization of $a(t)$ is arbitrary, and by convention its present value is set to

$$a(t_0) = 1. \tag{1.9}$$

This normalization is particularly useful because many cosmological observables (including the Hubble parameter $H(t) = \dot{a}/a$ and the redshift of distant sources) are defined in terms of the time evolution of the scale factor [4].

1.3 Dynamics of the universe: the Friedmann Equations

After introducing the metric of an expanding spacetime, it is possible to discuss its dynamical evolution and derive the laws that govern the behaviour of the scale factor $a(t)$.

The relation between spacetime geometry and its energy content is encoded in Einstein's field equation (EFE) [5]:

$$R_{\mu\nu} - \frac{1}{2} g_{\mu\nu} R = \frac{8\pi G}{c^4} T_{\mu\nu} \tag{1.10}$$

Here $R_{\mu\nu}$ denotes the Ricci tensor, defined as a contraction of the Riemann tensor and which describes the local geodesic deviation; $R = g^{\mu\nu} R_{\mu\nu}$ is the Ricci scalar, which measures the average curvature associated with the metric $g_{\mu\nu}$.

The EFE follows from the Einstein–Hilbert action,

$$S_{\text{EH}} = \frac{c^3}{16\pi G} \int d^4x \, \sqrt{-g} \, R, \tag{1.11}$$

whose Lagrangian density satisfies the physical criteria imposed by General Relativity: covariance under general coordinate transformations, locality, equations of motion involving at most first derivatives of the metric, and consistency with Newtonian gravity in the appropriate limit.

Because Einstein's equations consist of ten coupled second-order differential equations, exact solutions exist only in cases of high symmetry. Relevant examples for cosmology are Minkowski spacetime ($R = 0$, $k = 0$), de Sitter spacetime ($R > 0$, $k = +1$), anti–de Sitter spacetime ($R < 0$, $k = -1$), and the Friedmann solution (regarding a perfect fluid).

To apply the EFE in a cosmological setting, one substitutes the FLRW metric into the definitions of the Ricci tensor and scalar:

$$R_{\mu\nu} = \partial_\lambda \Gamma^\lambda_{\mu\nu} - \partial_\nu \Gamma^\lambda_{\mu\lambda} + \Gamma^\lambda_{\lambda\rho}\Gamma^\rho_{\mu\nu} - \Gamma^\lambda_{\nu\rho}\Gamma^\rho_{\mu\lambda}, \qquad R = g^{\mu\nu}R_{\mu\nu}. \tag{1.12}$$

Inserting the FLRW metric yields the non-vanishing components

$$R_{00} = -3\,\frac{\ddot{a}}{a}, \qquad R_{ij} = g_{ij}\left(\frac{\ddot{a}}{a} + 2H^2\right), \tag{1.13}$$

and the Ricci scalar

$$R = 6\left(\frac{\ddot{a}}{a} + H^2\right). \tag{1.14}$$

(where both 1.13 and 1.14 hold when k=0)

To determine the right-hand side of the EFE, the matter content of the Universe is modelled as a perfect fluid [6]:

$$T_{\mu\nu} = (\rho c^2 + P)\, u_\mu u_\nu + P\, g_{\mu\nu}, \tag{1.15}$$

where $\rho(t)$ is the energy density, $P(t)$ the isotropic pressure, and u^μ the quadrivelocity for a comoving observer.

The thermodynamic properties of the cosmic fluid are encoded in a linear equation of state,

$$P(t) = c^2 \omega(t)\, \rho(t), \tag{1.16}$$

with $\omega(t)$ approximately constant during a given cosmological era: $\omega = 0$ for pressureless matter, $\omega = \frac{1}{3}$ for radiation, $\omega = -1$ for a cosmological constant.

The local conservation of the energy–momentum tensor,

$$\nabla_\mu T^{\mu\nu} = 0, \tag{1.17}$$

leads to the continuity equation

$$\dot{\rho} + 3H(\rho + \frac{P}{c^2}) = 0. \tag{1.18}$$

Combining this with the equation of state gives

$$\rho(a) \propto a^{-3(1+\omega)}. \tag{1.19}$$

Since each cosmological component scales differently with the expansion, the Universe has passed through phases in which a single component dominated the total energy density:

$$\rho \propto a^{-4} \quad \text{(radiation)}, \qquad \rho \propto a^{-3} \quad \text{(matter)}, \qquad \rho = \text{const.} \quad (\Lambda).$$

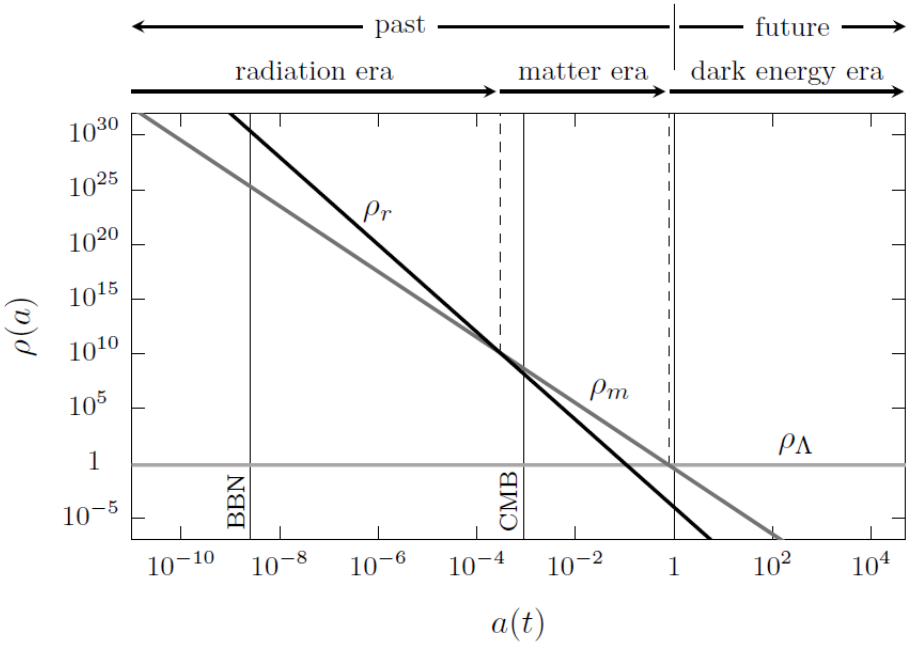


Figure 1.1: Evolution of the energy densities of the universe's constituents as a function of the scale factor a. The plot illustrates the succession of cosmological eras characterized by a single dominant component: the radiation-dominated era ($\rho_r \propto a^{-4}$), the matter-dominated era ($\rho_m \propto a^{-3}$), and the current dark-energy-dominated era ($\rho_\Lambda \sim$ const). The transition phases occur when the densities of the competing components are comparable. Figure adapted from Ref. [4].

Substituting the FLRW expressions for $R_{\mu\nu}$ and the perfect-fluid form of $T_{\mu\nu}$ into the field equation gives the two Friedmann equations:

$$H^2 = \left(\frac{\dot{a}}{a}\right)^2 = \frac{8\pi G}{3}\rho - \frac{kc^2}{a^2 R_0^2} + \frac{\Lambda c^2}{3}, \tag{1.20}$$

$$\frac{\ddot{a}}{a} = -\frac{4\pi G}{3}\left(\rho + 3\frac{P}{c^2}\right) + \frac{\Lambda c^2}{3}. \tag{1.21}$$

It is useful to introduce the critical density

$$\rho_c(t) = \frac{3H^2(t)}{8\pi G}, \tag{1.22}$$

the corresponding density parameter

$$\Omega(t) = \frac{\rho(t)}{\rho_c(t)}, \tag{1.23}$$

and the curvature parameter

$$\Omega_k(t) = 1 - \Omega(t) = \frac{(a_0 H_0)^2}{(aH)^2}\Omega_{k,0} \tag{1.24}$$

Assuming $a(t_0) = 1$ today, the first Friedmann equation can be written in reduced form, with each cosmological component contributing through its own density parameter:

$$\Omega_r + \Omega_m + \Omega_\Lambda + \Omega_k = 1 \tag{1.25}$$

When the Universe is flat and dominated by a single fluid, the scale factor admits exact solutions:

$$a(t) \propto t^{1/2} \qquad \text{(radiation era)},$$

$$a(t) \propto t^{2/3} \qquad \text{(matter era)},$$

$$a(t) \propto e^{Ht} \qquad (\Lambda\text{-dominated era}).$$

These expressions describe the expansion history during the main cosmological epochs.

1.4 Problems of the Big Bang model and introduction to inflation

Even though the hot Big Bang scenario is the benchmark model for the early Universe, and it successfully describes cosmic evolution back to roughly one second after the beginning, it still leaves three striking features of our Universe unexplained. These issues cannot be dismissed as simple coincidences and are traditionally referred to as the *problems of the hot Big Bang model* [4, 1, 2].

Horizon problem. The remarkable uniformity of the Cosmic Microwave Background (CMB) indicates that regions of the sky that are causally disconnected -that is, separated by more than the particle horizon at recombination- share almost exactly the same temperature, with fluctuations of order 10^{-5}. In the standard Big Bang picture there is no reason for such distant regions, whose past light cones never overlapped, to have physical conditions related to this accuracy level.

Flatness problem. Current observations constrain the spatial curvature to be extremely small, with $|1 - \Omega_0| \leq 10^{-3}$. However, in a Universe evolving under the standard Big Bang dynamics, even the tiniest initial deviation from flatness would grow enormously over cosmic time. This implies that the early Universe had to begin with an almost perfectly flat spatial curvature.

Monopole problem. Grand Unified Theories (GUTs) predict the production of magnetic monopoles as relics of the phase transition that broke the symmetry between strong and electroweak forces. Such transitions should produce roughly one monopole per Hubble volume, yet no magnetic monopole has ever been observed.

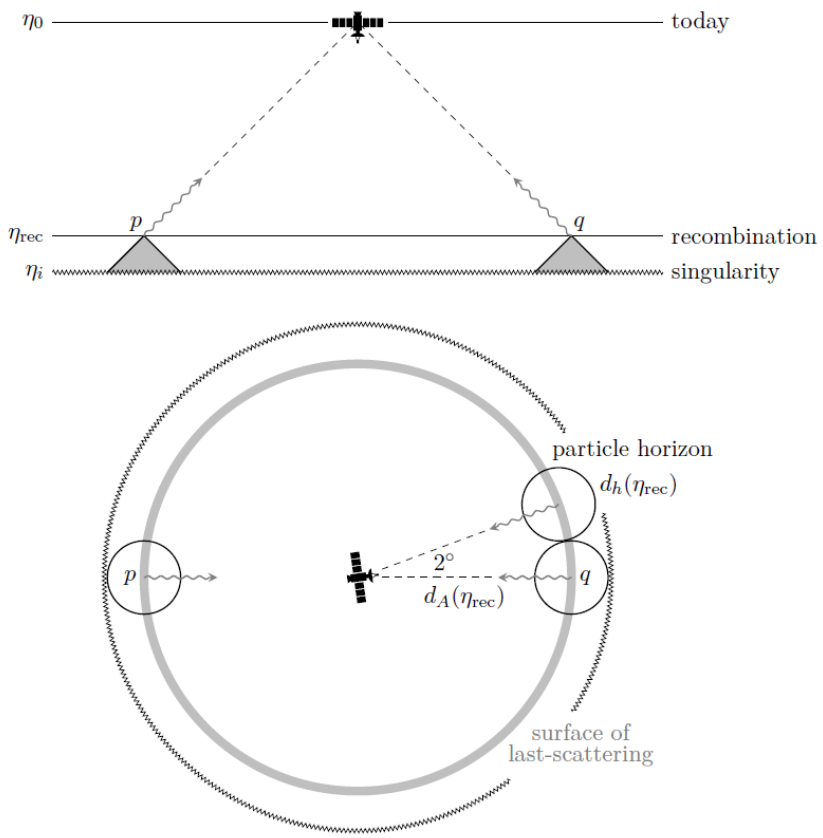


Figure 1.2: Schematic representation of the horizon problem in the conventional Big Bang model. The observer's past light cone intersects the spacelike hypersurface at the time of recombination, thereby defining the surface of last scattering. Points separated by an angular distance larger than $\sim 2^\circ$ on the sky possess non-overlapping past light cones, implying they could not have been in causal contact. Figure adapted from Ref. [4]

.

A single physical mechanism capable of simultaneously addressing these inconsistencies was proposed by Alan Guth in 1981: the idea that the entire observable Universe originated from a very small, causally connected region that underwent a phase of rapid, almost-exponential expansion. This stage is known as *cosmic inflation*.

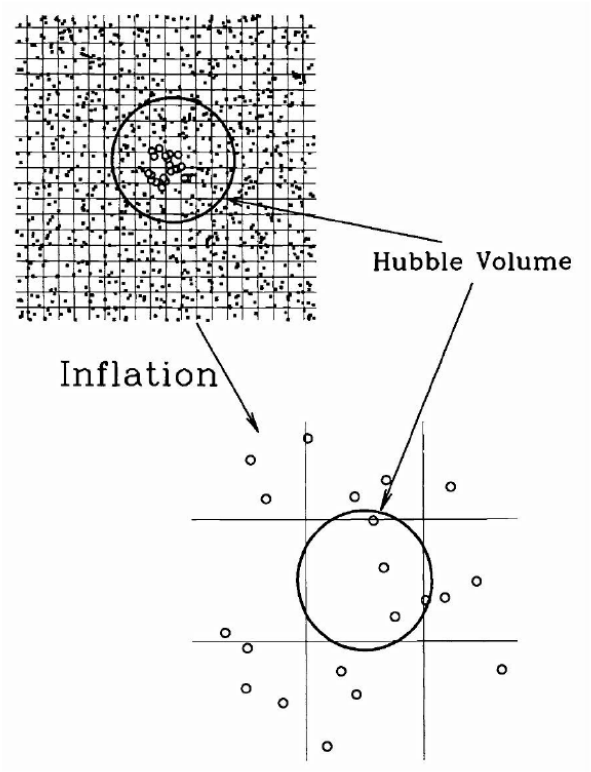


Figure 1.3: Intuitive depiction of the accelerated expansion occurring during the inflationary epoch. The background grid represents the comoving coordinate system, tracking the evolution of the scale factor a(t), while the solid circles represent the comoving Hubble radius $(aH)^{-}1$ before and after inflation. As the Universe undergoes a phase of exponential expansion, the comoving Hubble sphere shrinks dramatically. Consequently, a region that initially contained multiple grid patches (causally connected) is stretched to such an extent that a single patch vastly exceeds the size of the post-inflationary Hubble volume. Figure adapted from [7].

An accelerated expansion is characterized by

$$\ddot{a} > 0.$$

Using the second Friedmann equation,

$$\frac{\ddot{a}}{a} = -\frac{4\pi G}{3}(\rho + 3\frac{P}{c^2}),$$

we see that $\ddot{a} > 0$ requires

$$P < -\frac{\rho c^2}{3}, \tag{1.26}$$

which corresponds to an equation-of-state parameter $\omega = P/\rho < -1/3$.

Inflation was therefore produced by a source of negative pressure, acting as a repulsive gravity. Today, such a component is known as dark energy and is often modeled, at the background level, by a cosmological constant Λ. However, the value of Λ necessary to produce the inflationary expansion would have been enormously larger (by roughly 10^{107} in magnitude) than the present-day dark energy density.

The duration of inflation is conveniently expressed through the number of e-folds,

$$N \equiv \ln\left(\frac{a(t_f)}{a(t_i)}\right) \tag{1.27}$$

Here, t_i and t_f denote the beginning and the end of the inflationary period. Guth originally identified t_i with the GUT epoch, $t_i \sim 10^{-36}\,\mathrm{s}$ [1]. To match observations, roughly $N \simeq 60$ are required, corresponding to an expansion factor of $a(t_f)/a(t_i) \sim e^{60} \sim 10^{26}$.

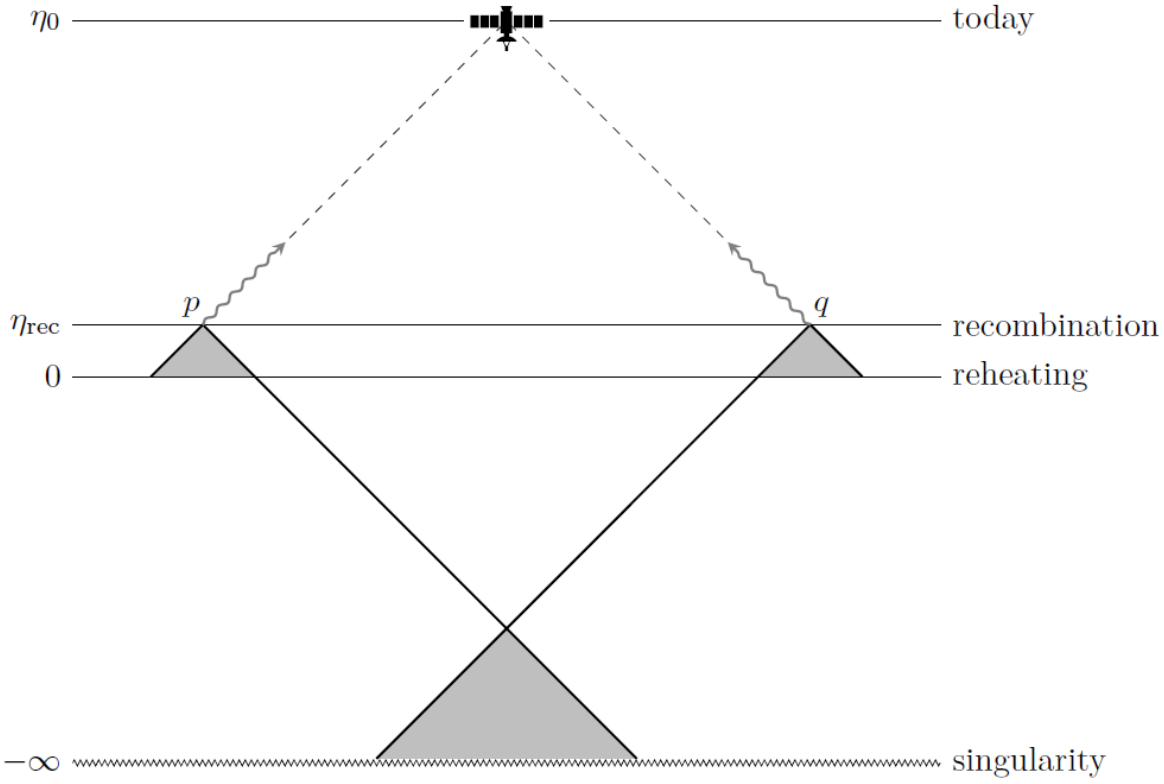


Figure 1.4: Kinematic solution to the cosmological horizon problem via inflation. By introducing a phase of accelerated expansion, the initial singularity is pushed to negative conformal time ($\eta \to -\infty$), drastically extending the causal history of the Universe. The surface $\eta = 0$ now defines the reheating transition rather than the absolute origin of time. Thanks to this extended pre-Big Bang epoch, the past light cones of any two seemingly disconnected points on the CMB sky inevitably intersect, providing a natural causal mechanism for the observed large-scale homogeneity. Credits: [4].

To understand how inflation resolves the problems of the Big Bang model, it is useful to recall three notions of cosmic horizons [5].

Particle horizon. This is a non-local quantity, determined by the entire past history of the scale factor:

$$d_{\rm particle}(t) = a(t) \int_0^t \frac{c\, dt'}{a(t')}. \tag{1.28}$$

It represents the maximum comoving distance from which light could have reached an observer by the time t; equivalently, it separates regions that have ever been in causal contact from those that have not.

Hubble radius. The Hubble scale,

$$R_H(t) = \frac{1}{H(t)}, \tag{1.29}$$

characterizes the local expansion rate. It separates perturbation modes with wavelengths smaller or larger than the Hubble radius (sub- and super-Hubble modes). Points separated by more than $R_H(t)$ recede from one another faster than the speed of light due to cosmic expansion; this, however, is *not* a causal horizon.

Event horizon. This is defined as

$$d_{\rm event}(t) = a(t) \int_t^\infty \frac{c\, dt'}{a(t')}, \tag{1.30}$$

and depends on the entire future evolution of the scale factor. In an accelerating Universe, the integral converges, meaning that there exist regions from which light emitted now will never reach us.

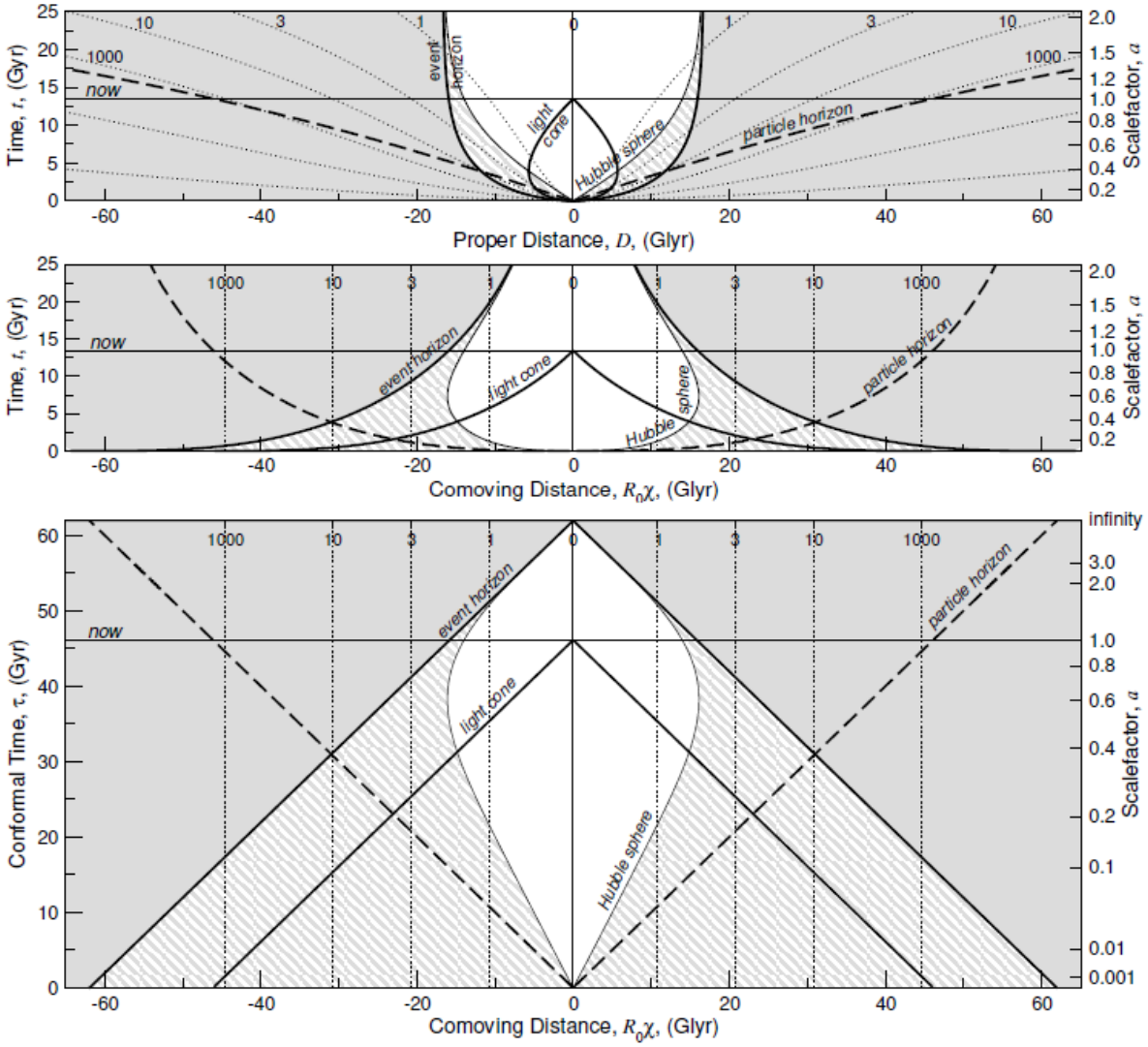


Figure 1.5: Comparison of spacetime diagrams in proper distance (top), comoving coordinates (middle), and conformal coordinates (bottom) for a concordance ΛCDM model. The panels depict the worldlines of comoving objects (dotted lines) relative to our central observer position, along with our past light cone. Key cosmological boundaries are shown: the Hubble sphere (thin solid line), the particle horizon (dashed line), and the event horizon. The conformal diagram in the lower panel is particularly illuminating, as it maps the entire cosmic history into a finite vertical domain, revealing that light travelling since the Big Bang ($t = 0$) originated from a finite comoving distance of roughly 46 Glyr, defining our current observable Universe. Credits: [8].

The key distinction between these concepts is that an object outside the Hubble radius is out of causal contact *now*, whereas an object outside the particle horizon has *never* been in causal contact.

During inflation, the particle horizon grows rapidly, while the Hubble radius shrinks.

As a result, many regions that appear causally disconnected today actually shared overlapping past light cones during the inflationary era [4].

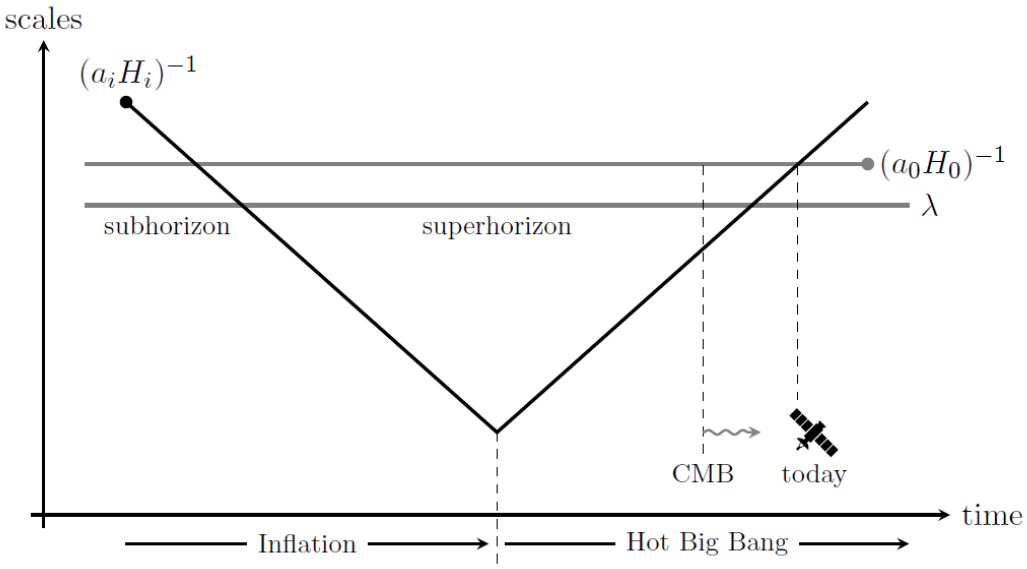


Figure 1.6: The plot illustrates the evolution of a representative fluctuation of fixed comoving wavelength relative to the comoving Hubble radius $(aH)^{=1}$, demonstrating the inflationary solution to the super-horizon correlations problem. While this mode appears to be outside the causal horizon at the time of Cosmic Microwave Background (CMB) decoupling, the shrinking Hubble sphere during inflation ensures that it was initially sub-horizon. Microphysical causal processes could therefore generate the primordial correlations before the mode exited the horizon and froze, only to re-enter at late cosmological times. Figure adapted from Ref. [4].

The scale factor's growth trend during inflation resolves the flatness problem as well: since spatial curvature evolves as

$$\Omega_k(t) - 1 = \frac{kc^2}{a^2H^2}, \tag{1.31}$$

for an approximately exponential expansion, $a(t) \propto e^{Ht}$, and a nearly constant H, one finds

$$|\Omega_k(t) - 1| \propto e^{-2Ht}.$$

Thus, even if the Universe had been significantly curved prior to inflation, the curvature term would have been exponentially suppressed by the end of the inflationary stage.

To this day, the exact physics behind the driving mechanism of inflation is not known.

Most of the acknowledged theories achieve an almost-exponential expansion through a homogeneous scalar field $\phi(t)$, the *inflaton* [2].

The action for a minimally coupled scalar field is[1]

$$S = \int d^4x \sqrt{-g} \left[\frac{1}{2} g^{\mu\nu} \partial_\mu \phi \, \partial_\nu \phi - V(\phi) \right], \tag{1.32}$$

Variation with respect to ϕ gives the Klein–Gordon equation in an expanding background:

$$\ddot{\phi} + 3H\dot{\phi} + V'(\phi) = 0, \tag{1.33}$$

where the term $3H\dot{\phi}$ acts as a damping term, often called *Hubble friction*.

In natural units, the energy density and pressure associated with ϕ are

$$\rho_\phi = \frac{1}{2}\dot{\phi}^2 + V(\phi), \qquad P_\phi = \frac{1}{2}\dot{\phi}^2 - V(\phi), \tag{1.34}$$

Inflation occurs when the field's potential energy dominates $\dot{\phi}^2 \ll V(\phi)$, implying $P_\phi \approx -\rho_\phi$ and $\omega_\phi \approx -1$: the inflaton is then acting as a cosmological constant, and can elicit an accelerated expansion.

Guth's first proposal was a scalar field trapped in a local minimum of its potential, a false vacuum, for the duration of the inflationary period; this configuration is metastable since quantum tunneling can happen, putting the field at its global minimum (true vacuum). This first order phase transition would end the universe's exponential expansion, but this scenario does not successfully end inflation. A more fruitful idea is *slow-roll inflation*, in which the field rolls gradually along a sufficiently flat region of its potential towards its true minimum. This formalism is today the standard framework for the most debated models (Chaotic inflation, natural inflation, Starobinsky, ...).

[1] in natural units $\hbar = c = 1$

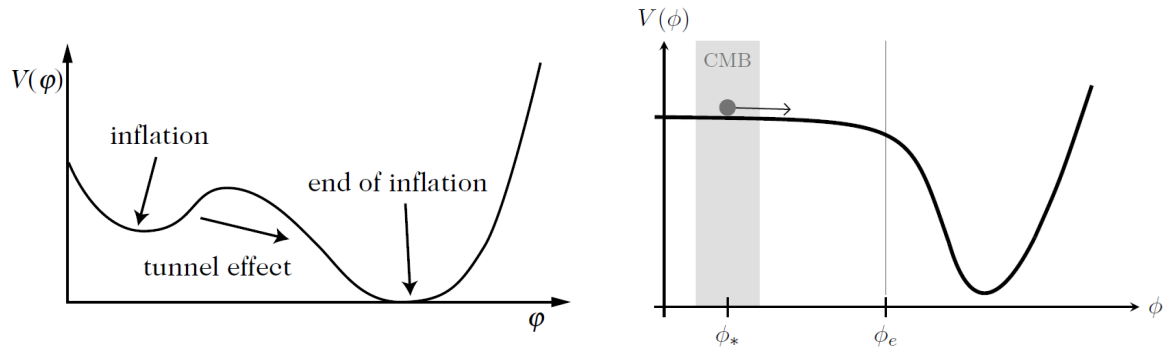


Figure 1.7: Evolution of the inflationary paradigm. The left panel illustrates Guth's "old inflation," relying on a first-order phase transition from a local false vacuum to a true minimum via quantum tunneling. This scenario historically suffered from the "graceful exit" problem, as the bubbles of true vacuum could not percolate fast enough to end inflation homogeneously. The right panel depicts "new inflation," wherein the scalar field slowly relaxes towards its true vacuum over a shallow potential energy plateau. This continuous slow-roll dynamics naturally provides a mechanism to successfully end the accelerated expansion and initiate reheating. Credits: [2, 4].

The conditions for slow roll can be expressed through the slow-roll parameters:

$$\begin{aligned} \epsilon_H &= -\frac{\dot{H}}{H^2}, \qquad \eta_H = -\frac{\ddot{\phi}}{H\dot{\phi}} \qquad \text{(Hubble } H \text{ slow-roll parameters)} \\ \epsilon_V &= \frac{M_{\rm Pl}^2}{2}\left(\frac{V'}{V}\right)^2, \quad \eta_V = M_{\rm Pl}^2\frac{V''}{V} \qquad \text{(Potential } V(\phi) \text{ slow-roll parameters)} \end{aligned} \tag{1.35}$$

where M_{Pl} is the reduced Planck mass, and primes denote derivatives with respect to the field ϕ

Inflation requires $\epsilon_H < 1$, and the slow-roll regime holds when $\epsilon_V \ll 1$ and $|\eta_V| \ll 1$ [1].

After leaving the slow-roll region, ϕ oscillates around the minimum of its potential. These oscillations lead to the transfer of energy from the inflaton field to standard particles and radiation, a process known as *reheating* [6]. Reheating connects the end of the accelerated phase to the familiar radiation-dominated era, restoring the high-temperature conditions required by the hot Big Bang framework.

Chapter 2

A BRIEF INTRODUCTION TO GRAVITATIONAL WAVES

Gravitational waves (GWs) represent an exceptional tool for observing the primordial Universe: as weakly interacting messengers, they decouple almost immediately upon production, propagating freely through cosmic history while maintaining their spectral information [9].

In this chapter, we focus on the classical description of GWs in General Relativity and their propagation, without addressing their physical origin; the mechanisms responsible for their generation, particularly during the inflationary era, will be addressed in Chapter 3.

2.1 Gravitational waves in General Relativity

To define GWs mathematically, we start from the Einstein field equations [1.10]. This form of the field equation is obtained by requiring the theory to reduce to the Newtonian limit in the weak-field case, meaning spacetime is nearly flat. In this regime, we can operate a perturbative decomposition of the metric [2]:

$$g_{\alpha\beta} = \bar{g}_{\alpha\beta} + \delta g_{\alpha\beta} \tag{2.1}$$

where $\bar{g}_{\alpha\beta}$ is the unperturbed background metric and $\delta g_{\alpha\beta}$ is a small perturbation.

The most natural approach to introduce gravitational waves is to consider the weak-field limit in the simplest possible case, namely when the background metric $\bar{g}_{\alpha\beta}$ is chosen to be the Minkowski metric $\eta_{\mu\nu}$. Moreover, since the observable amplitudes of gravitational waves

are extremely small, the analysis can be further simplified by expanding Einstein's equations to first order in the perturbation, obtaining the linearized theory of General Relativity. In this framework, we adopt the notation

$$g_{\mu\nu} = \eta_{\mu\nu} + h_{\mu\nu}(x) \tag{2.2}$$

where $|h_{\mu\nu}| \ll 1$ represents the metric perturbation.[1]

Gauge Freedom and the Lorenz Gauge

At this stage, it is essential to recall that the form of the metric perturbation is not unique but depends on the reference frame. Gravitational waves, however, represent a physical phenomenon and must therefore be independent of coordinate choice and must be described by the gauge-invariant content of the metric perturbation.

In order to extract the propagating wave solutions expected from a second-order differential field equation in space and time, it is necessary to operate gauge choices that eliminate the spurious degrees of freedom associated with coordinate ambiguities. In General Relativity, two perturbations describing the same physical spacetime are related by an infinitesimal coordinate transformation,

$$x^\mu \to x'^\mu = x^\mu + \xi^\mu(x) \tag{2.3}$$

under which the metric perturbation transforms accordingly as

$$h_{\mu\nu} \to h'_{\mu\nu} = h_{\mu\nu} - \partial_\mu \xi_\nu - \partial_\nu \xi_\mu \tag{2.4}$$

Exploiting the freedom in choosing ξ_μ, we can impose the gauge condition:

$$\partial^\nu \bar{h}_{\mu\nu} = 0 \tag{2.5}$$

where $\bar{h}_{\mu\nu} = h_{\mu\nu} - \frac{1}{2}\eta_{\mu\nu}h$ is the trace-reversed perturbation. This is generally called the harmonic or de Donder gauge, which reduces to the Lorenz gauge in flat spacetime [10].

This gauge condition imposes four constraints that reduce the independent components of $h_{\mu\nu}$ from 10 to 6; as a consequence, the linearized field equations reduce to a simple wave

[1] This choice implicitly assumes a coordinate system valid over a sufficiently large region of space.

equation:

$$\Box \bar{h}_{\mu\nu} = -\frac{16\pi G}{c^4} T_{\mu\nu} \tag{2.6}$$

In vacuum, where $T_{\mu\nu} = 0$, this equation describes freely propagating waves traveling at the speed of light.

SVT decomposition and gauge invariance

Before imposing further gauge conditions, it is convenient to introduce a classification of metric perturbations that is independent of the gauge choice: this classification emerges from their transformation properties under spatial rotations, and reflects the symmetries of a homogeneous and isotropic background. Perturbations are naturally decomposed into scalars, vectors, and tensors (SVT decomposition), which evolve independently at first order and can therefore be treated separately. The ten degrees of freedom of the metric perturbation are decomposed into:

- **4 scalar functions** (A, B, ψ, E);
- **2 vector functions** (S_i, F_i);
- **1 tensor function** (E_{ij}).

While tensors are intrinsically gauge-invariant, this is not true for scalar and vector functions. It follows that GWs are uniquely described, at linear order, by the tensor component, which remains identical in all frames of reference. Vector perturbations will not be discussed in this dissertation, since any such modes produced during inflation would decay rapidly with the expansion of the Universe. Scalar perturbations, on the other hand, can be treated using the gauge-invariant variables, such as the Bardeen potentials, which will be introduced later in Chapter 3, in the context of second-order sources of gravitational waves.

Transverse-traceless gauge and physical polarizations

After fixing the Lorenz gauge, $h_{\mu\nu}$ still possesses a residual gauge freedom (associated with infinitesimal coordinate transformations) that preserve the gauge condition.

Choosing the four functions ξ_μ that satisfy $\Box\xi_\mu = 0$ to impose four additional conditions saturates the residual gauge freedom, and leads to the transverse-traceless (TT) gauge [10, 4]:

$$h^{0\mu} = 0, \tag{2.7}$$

$$\partial^i h_{ij} = 0, \tag{2.8}$$

$$h^i{}_i = 0. \tag{2.9}$$

This set of conditions eliminates coordinate redundancy, revealing that gravitational waves have no temporal components (2.7) and produce only transverse (2.8), traceless (2.9) spatial distortions: the "traceless" condition indicates that gravitational waves cause anisotropic distortions (pure shear deformations that preserve local volumes), while the "transverse" condition means GWs only have non-vanishing components in the plane normal to propagation. In the TT gauge, the metric perturbation contains only two[2] independent components, corresponding to the two amplitudes of the physical polarization states of the gravitational wave: these are commonly denoted as h_+ and $h_\times$. Choosing the propagation direction along the z-axis, the perturbation takes the standard form

$$h_{ij}^{\mathrm{TT}}(t,z) = \begin{pmatrix} h_+ & h_\times & 0 \\ h_\times & -h_+ & 0 \\ 0 & 0 & 0 \end{pmatrix}. \tag{2.10}$$

2.2 Observational and physical properties of GWs

Having defined GWs at a theoretical level, we now focus on their observable and physical properties, discussing how they interact with matter and which measurable quantities allow for their experimental detection.

[2]The degree-of-freedom count is thus $10(\text{total}) - 4(\text{Lorenz}) - 4(\text{residual}) = 2$

Geodesic deviation

We start by recalling the equation describing the motion of a mass in a curved background which, in the absence of non-gravitational forces, follows a geodesic path. Consider two nearby geodesics $x^\mu(\tau)$ and $x^\mu(\tau) + n^\mu(\tau)$, where $n^\mu(\tau)$ denotes their separation vector. The relative acceleration between the two worldlines is governed by the geodesic deviation equation,

$$\frac{D^2 n^\mu}{d\tau^2} = -R^\mu{}_{\nu\rho\sigma} u^\nu u^\rho n^\sigma \tag{2.11}$$

where u^μ is the four-velocity along the reference geodesic and $R^\mu{}_{\nu\alpha\beta}$ is the Riemann curvature tensor. This equation describes the tidal acceleration between nearby geodesics due to spacetime curvature. This effect is not caused by a force, but is entirely determined by the Riemann tensor, making it gauge-invariant within linearized gravity [9]. If the spacetime curvature is produced by the passage of a gravitational wave, the relevant components of the Riemann tensor can be expressed in terms of the transverse-traceless metric perturbation. In the proper detector frame, one finds

$$R_{0i0j} = -\frac{1}{2}\,\ddot{h}^{\mathrm{TT}}_{ij}, \tag{2.12}$$

so that the spatial component n^i of n^σ in the geodesic deviation equation reduce to

$$\ddot{n}^i = \frac{1}{2}\,\ddot{h}^{\mathrm{TT}}_{ij}\, n^j \tag{2.13}$$

This relation shows how physical distances oscillate due to the passing of the wave, that induces tidal accelerations proportional to the second time derivative of its amplitude. Although this equation formally resembles Newton's second law, the acceleration does not originate from a physical force, but from spacetime curvature. Nevertheless, this analogy provides an intuitive description of the effect of gravitational waves on terrestrial detectors, which will be discussed in Chapter 4.

The manifest effect of a GW on a test mass depends on the chosen coordinates. In the TT gauge (comoving coordinates), the wave does not affect the positions of the masses: particles at rest before the wave's arrival remain at fixed spatial coordinates, while physical distances oscillate due to the time-dependent metric. In contrast, in the proper detector frame the metric is locally Minkowskian, and the effect of the wave is described in terms of the relative motion

of the test masses [10]. To appreciate this gauge-invariant physical effect, it is therefore necessary to consider the relative behavior of at least two particles; moreover, since the imprint of a gravitational wave on matter is not detected through absolute displacements, but through relative variations of distances, it is convenient to introduce a fundamental observational parameter: the gravitational-wave strain h.

$$h \equiv \frac{\Delta L}{L}, \tag{2.14}$$

This dimensionless quantity is a measure of the relative variation ΔL of a proper distance L due to the passage of the wave.

A classic example that captures how a GW affects masses consists of a ring of freely falling particles, initially at rest in the proper detector frame. A gravitational wave propagating along the normal direction to the plane containing the masses causes the ring to stretch along one axis and compress along the orthogonal one, maintaining a constant area (which reflects the traceless nature of the perturbation). The two independent polarizations, h_+ and $h_\times$, give rise to the same pattern, rotated by 45° with respect to each other.

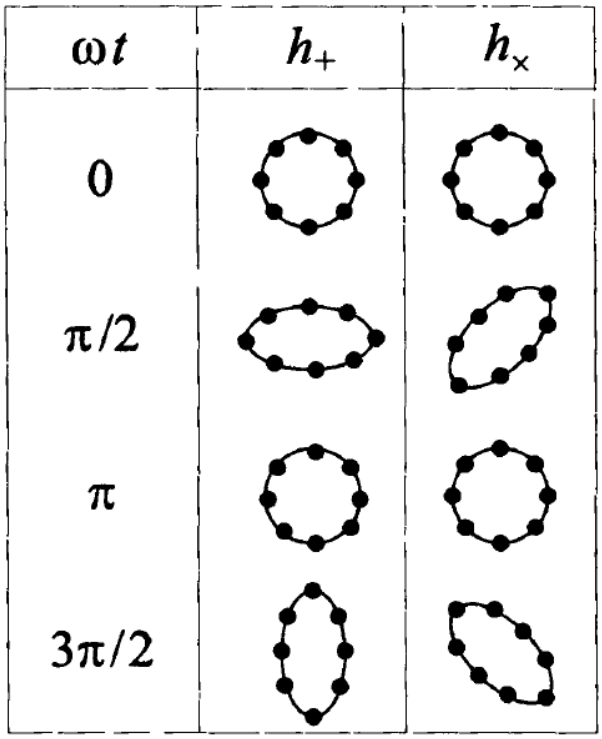


Figure 2.1: Physical effect of a passing gravitational wave on a circular ring of freely falling test masses in the transverse plane. The "plus" (+) polarization state induces an oscillating tidal deformation along the x and y axes. The "cross" (×) polarization state generates an analogous deformation pattern, but rotated by 45°. This transverse, quadrupolar stretching and squeezing of spacetime is a fundamental signature of gravitational radiation in General Relativity. Adapted from [10].

2.3 Gravitational Waves in FLRW background

Until now, we have assumed a Minkowski background for simplicity, which allowed us to observe how perturbations in flat space satisfy a standard wave equation in the appropriate gauge. However, in a real cosmological context, GWs evolve in the curved and expanding background described by the Friedmann-Lemaître-Robertson-Walker (FLRW) metric we introduced in Chapter 1. It is therefore necessary to extend the definition of GWs to a generic dynamic and curved background metric $\bar{g}_{\mu\nu}$. Moving beyond Minkowski allows us to study how GWs act as a source of spacetime curvature, but it poses a non-trivial problem; namely that time dependence, previously confined to the perturbation, now also appears in the background metric: this makes it impossible to explicitly distinguish between the two as we did in flat space. Since there is no unique and covariant way to separate the "pure" metric from the perturbation, we use the separation of scales between the background (low frequency) and the waves (high frequency) [5, 9].

We can distinguish them if the wavelength and the background variation scale satisfy:

$$\lambda \ll L_B \quad \text{or}^{\,3} \quad f \gg f_B \tag{2.15}$$

The Isaacson tensor and energy density

To study the propagation of the perturbation $h_{\mu\nu}$ under these hypotheses, it is convenient to use the trace-reversed form of the Einstein field equations (eq. 1.10):

$$R_{\mu\nu} = \frac{8\pi G}{c^4}\left(T_{\mu\nu} - \frac{1}{2}g_{\mu\nu}T\right) \tag{2.16}$$

By expanding the Ricci tensor up to the second order, $R_{\mu\nu} \simeq \bar{R}_{\mu\nu} + R^{(1)}_{\mu\nu} + R^{(2)}_{\mu\nu}$, we can decompose the field equations into different frequency contributions: the first-order term $R^{(1)}_{\mu\nu}$ contains only high-frequency modes, while the second-order term $R^{(2)}_{\mu\nu}$ contains both.

[3] In GR, spatial and temporal scales are not necessarily linked. A blatant example is a neutron star: its gravitational field is approximately static ($f_B \approx 0$) but extremely curved (L_B is small). Fulfilling either condition is sufficient for scale separation.

To isolate the background, we perform an averaging procedure over an intermediate scale l ($\lambda \ll l \ll L_B$). This operation, often termed coarse-graining, causes rapid oscillations to average to zero, determining the background dynamics as:

$$\bar{G}_{\mu\nu} = \frac{8\pi G}{c^4}(\bar{T}_{\mu\nu} + t_{\mu\nu}) \tag{2.17}$$

where $\bar{G}_{\mu\nu}$ is the Einstein tensor constructed from the slowly varying background metric $\bar{g}_{\mu\nu}$, $\bar{T}_{\mu\nu} \equiv \langle T_{\mu\nu} \rangle$ represents the effective, coarse-grained energy-momentum tensor of the background matter fields, and $t_{\mu\nu}$ arises from the averaging of the terms quadratic in the high-frequency metric perturbations $h_{\mu\nu}$, and acts as the effective energy-momentum tensor of the gravitational waves themselves.

A particularly remarkable implication of this result is that the contribution of a gravitational wave to the curvature of spacetime is formally equivalent to that of a matter source with an associated energy-momentum tensor $t^{\mu\nu}$:

$$t_{\mu\nu} = \frac{c^4}{32\pi G} \left\langle \partial_\mu h_{\alpha\beta}\, \partial_\nu h^{\alpha\beta} \right\rangle . \tag{2.18}$$

This effective energy-momentum tensor, commonly referred to as the Isaacson tensor, arises from the averaged second-order contribution to the Ricci tensor in the high-frequency limit. In this regime, gravitational waves can be consistently treated as short-wavelength perturbations propagating on a slowly varying background, and the low-frequency component of the second-order curvature acts as a source for the background dynamics [9, 11].

From this expression one can directly extract two physical quantities of primary importance for gravitational-wave observations: the energy density carried by the wave, and the associated energy flux; in the TT gauge, these quantities are given by:

$$\rho_{GW} = \frac{c^2}{32\pi G}\langle \dot{h}ij\dot{h}^{ij} \rangle, \qquad F_{GW} = c\langle t_{0r} \rangle \tag{2.19}$$

Evolution in FLRW

In a flat FLRW metric, using conformal time , the perturbed line element is

$$ds^2 = a^2(\tau)\left[-d\tau^2 + (\delta_{ij} + h_{ij})dx^i dx^j\right] \tag{2.20}$$

Using the TT gauge to isolate tensor degrees of freedom, and moving to Fourier space, the evolution of a mode $h_k(\tau)$ with comoving wavevector k is governed by:

$$h_k'' + 2\mathcal{H}h_k' + k^2 h_k = \frac{16\pi G a^2}{c^4}\Pi_k^{TT} \tag{2.21}$$

where $\mathcal{H} = a'/a$ is the conformal Hubble parameter and Π_k^{TT} represents the anisotropic stress source. In the absence of sources, this takes the form of a damped harmonic oscillator, where the $2\mathcal{H}h_k'$ term acts as "Hubble friction" due to the expansion of the universe:

$$h_k'' + 2\mathcal{H}h_k' + k^2 h_k = 0 \tag{2.22}$$

The resulting behavior depends on the ratio between the wave's scale and the Hubble radius [9, 12]: the two possible qualitative regimes are

- **Sub-horizon ($k \gg \mathcal{H}$):** The k^2 term dominates (the amplitude is damped by the expansion). The solution behaves as

  $$h_k \propto a^{-1} e^{\pm ik\eta} \tag{2.23}$$

  The energy density scales as $\rho_{GW} \propto a^{-4}$, confirming that GWs propagate as radiation.

- **Super-horizon ($k \ll \mathcal{H}$):** The friction term dominates, leading to $h_k \approx$ const: after exiting the horizon, the GW amplitude remains "frozen"[4].

[4] This frozen state is fundamental for inflation, as it preserves primordial fluctuations to be discussed in Chapter 3.

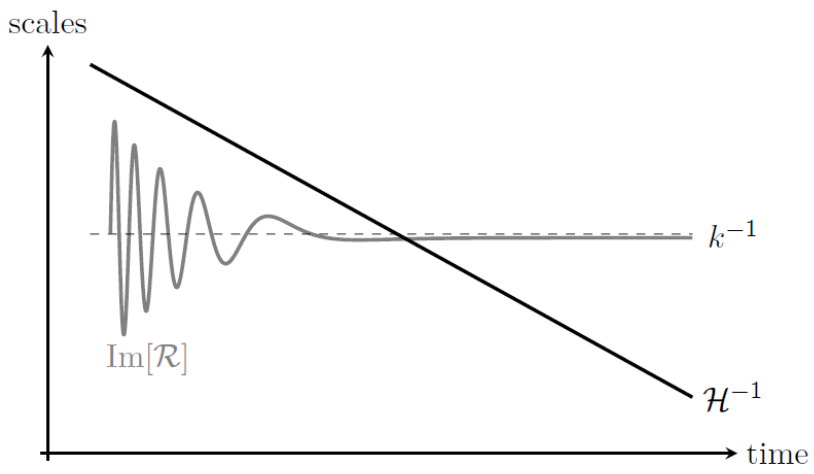


Figure 2.2: Qualitative evolution of a single Fourier mode across the Hubble horizon. Although the figure explicitly illustrates the comoving scalar curvature perturbation $\mathcal{R}$, the tensor metric perturbation h_k exhibits the exact same dynamical behavior: the mode undergoes damped acoustic oscillations on sub-horizon scales and remains completely frozen at a constant value on super-horizon scales. Credits:[4].

Having established how Gravitational Waves propagate, influencing the metric and carrying energy density, we now turn to the mechanisms responsible for their generation in the early Universe.

Chapter 3

COSMOLOGICAL PRODUCTION OF GRAVITATIONAL WAVES

3.1 Introduction: the quantum nature of perturbations

In the first chapter, we introduced cosmic inflation primarily as the mechanism required to resolve the major flaws of the standard Hot Big Bang model, such as the horizon and flatness problems. Although this provided the original theoretical motivation, it was soon realized that an inevitable and arguably more profound outcome of an accelerated expansion phase is the generation of primordial fluctuations, resulting in two distinct types of perturbations [13, 14, 15, 4]:

1. **Scalar perturbations** that arise from quantum fluctuations of the scalar field (the inflaton) coupled with the metric. They induce density inhomogeneities which, upon re-entering the horizon, seed the formation of Large Scale Structures (LSS).

2. **Tensor perturbations** are sourced from the quantum fluctuations of the metric itself; unlike scalar perturbations that do not produce GWs, the superposition of tensor modes generates a stochastic background of primordial gravitational waves (SGWB).

While predictions regarding scalar modes have been confirmed with high precision by measurements of temperature anisotropies in the Cosmic Microwave Background (CMB) [6, 4],

the detection of the SGWB has not yet occurred. If we ever manage to discover it, it would provide insight on the physical mechanisms driving inflation and constrain its energy scale; furthermore, it would provide strong evidence in favor of the quantization of the gravitational field [10, 9].

This chapter, which constitutes the core of this thesis, is devoted to the study of the mechanisms responsible for the generation of a primordial background of gravitational waves. In particular, we focus on their quantum origin within the framework of single-field inflation in the slow-roll regime; going beyond the purely classical approach of General Relativity provided in the previous section, we will treat tensor perturbations as quantum fields evolving in a quasi-de Sitter expanding spacetime.

Introductory conceptual background: Quantum Field Theory

Before deriving the spectrum of primordial GWs, it is essential to summarize the fundamental premise of Quantum Field Theory. According to QFT, "fundamental entities are not particles, but the fields that permeate the universe: within this framework, a particle is just a quantum excitation of the corresponding fields.

For instance, an electron is not an isolated object, but a local expression of energy fluctuations of the fundamental electron field (Dirac field), just as a photon is a quantum of the electromagnetic field [4].

A crucial consequence of this description concerns the nature of the vacuum. When a quantum field is in its state of minimal energy (the *vacuum state*), due to the Heisenberg uncertainty principle, its value and its conjugate momentum cannot be simultaneously zero. Therefore, the vacuum does not correspond to absolute emptiness, but is characterized by continuous stochastic variations in energy, known as *zero-point fluctuations*.

In the context of the early Universe, these vacuum fluctuations play a dual role:

1. **Reheating and Matter Creation:** Since the vacuum is the seat of constant creation and annihilation of virtual particles, the rapid change in spacetime geometry during inflation can separate these pairs or transfer energy to them. This mechanism is fundamental to the *reheating* process, which converts the energy of the inflaton vacuum into the hot plasma of Standard Model particles required for the Hot Big Bang [12].

2. **Primordial GW Generation:** As we will demonstrate in the following, the inflationary expansion stretches microscopic quantum fluctuations of the metric to macroscopic scales. When the physical wavelength of these fluctuations exceeds the Hubble radius, they "freeze out" and are converted into classical tensor perturbations, which could be observed today as a background of gravitational waves [4, 9].

3.2 Quantization of tensor modes and graviton production

We now establish the theoretical formalism required to describe the quantum generation of primordial gravitational waves, considering linear perturbations h_{ij} on a spatially flat Friedmann-Lemaître-Robertson-Walker (FLRW) background; as discussed in Chapter 2, these perturbations are gauge-invariant, transverse, and traceless (when choosing the TT gauge). To quantize the system, we start by expanding the Einstein-Hilbert action to second order in h_{ij}, which in conformal time τ, is given by [9, 4]:

$$S_T^{(2)} = \frac{M_{Pl}^2}{8} \int d\tau d^3x \, a^2(\tau) \left[(h'_{ij})^2 - (\nabla h_{ij})^2 \right] , \tag{3.1}$$

where $M_{Pl} = \sqrt{\frac{\hbar c}{8\pi G}}$ is the reduced Planck mass, $a(\tau)$ is the scale factor, and primes denote derivatives with respect to conformal time. It is convenient to decompose the tensor field into its Fourier modes and polarization states; expanding $h_{ij}(\tau, \mathbf{x})$ in terms of the polarization tensors $\epsilon_{ij}^{(\lambda)}$ (with $\lambda = +, \times$):

$$h_{ij}(\tau, \mathbf{x}) = \sum_{\lambda} \int \frac{d^3k}{(2\pi)^3} h_{\mathbf{k},\lambda}(\tau) \epsilon_{ij}^{(\lambda)}(\mathbf{k}) e^{i\mathbf{k}\cdot\mathbf{x}} \tag{3.2}$$

The action for each polarization mode becomes formally equivalent to that of a massless scalar field in a curved background, up to an overall factor [9, 6]:

$$S_T^{(2)} = \sum_{\lambda=+,\times} \frac{M_{Pl}^2}{4} \int d\tau d^3k \, a^2(\tau) \left[|h'_{\mathbf{k},\lambda}|^2 - k^2 |h_{\mathbf{k},\lambda}|^2 \right] . \tag{3.3}$$

To proceed with canonical quantization, we introduce the **Mukhanov-Sasaki variable** $v_{\mathbf{k}}$, which absorbs the scale factor and normalizes the field [6, 12]:

$$v_{\mathbf{k},\lambda}(\tau) \equiv \frac{M_{Pl}}{2} a(\tau) h_{\mathbf{k},\lambda}(\tau) . \tag{3.4}$$

Substituting this variable into the action (3.3) and integrating by parts, the friction term (Hubble friction) is eliminated and the equation of motion for each mode $v_k(\tau)$ takes the form of a harmonic oscillator with a time-dependent effective mass:

$$v_k''(\tau) + \omega_k^2(\tau) v_k(\tau) = 0\,, \quad \text{with} \quad \omega_k^2(\tau) = k^2 - \frac{a''}{a}\,. \tag{3.5}$$

This equation, known as the Mukhanov-Sasaki equation, highlights the interaction between the tensor modes and the background geometry [4], with the term a''/a acting as a time-dependent potential induced by the expansion of the Universe.

We now promote the field variable v and its conjugate momentum $\pi = v'$ to quantum operators, imposing the standard relations [4, 9]:

$$\left[\hat{v}_{\mathbf{k},\lambda}(\tau), \hat{\pi}^\dagger_{\mathbf{q},\sigma}(\tau)\right] = i\delta_{\lambda\sigma}\delta^{(3)}(\mathbf{k}-\mathbf{q})\,. \tag{3.6}$$

A fundamental consequence of the relations 3.6 is that the field variance in the vacuum state $|0\rangle$ is non-zero, which confirms the existence of *zero-point fluctuations*:

$$\langle 0|\hat{v}^\dagger_{\mathbf{k}}\hat{v}_{\mathbf{k}}|0\rangle = |v_k(\tau)|^2 \neq 0\,. \tag{3.7}$$

Expanding the operator $\hat{v}_{\mathbf{k}}$ in terms of creation and annihilation operators, $\hat{a}_{\mathbf{k}}$ and $\hat{a}^\dagger_{\mathbf{k}}$, we can define the vacuum state $|0\rangle$ as the state annihilated by $\hat{a}_{\mathbf{k}}$ for all modes; however, in a time-dependent background such as the inflationary Universe, the definition of the vacuum is not unique, but depends on τ . Consequently, the state that minimizes the energy at an initial time τ_{in} ($|0\rangle_{in}$) is not the same state that minimizes the energy at a later time ($|0\rangle_{out}$) [10, 9]. This implies that, in the inflationary context, what appears as a vacuum state (having a null occupation number $n_k = 0$) to an observer at the beginning of inflation evolves into a multi-particle (excited) state with $n_k > 0$ for a later observer. Physically, the expansion of the Universe amplifies the zero-point fluctuations of the gravitational field and transforms them into a classical stochastic background of gravitational waves with a high occupation number of gravitons (squeezed state) [9, 5].

3.3 Primordial Perturbations from single-field slow-roll inflation

In the previous section, we illustrated the general procedure for the canonical quantization of tensor modes in an expanding background; we can now apply it to the specific case where the scalar field is the inflaton ϕ, defined in Chapter 1, and the evolution of the scale factor follows the slow-roll hypothesis. In this scenario, the Hubble parameter H is not strictly constant—otherwise inflation would never end—but varies very slowly ($|\dot{H}|/H^2 \ll 1$), corresponding to a quasi-de Sitter spacetime.

Recalling the expressions that defined the slow-roll condition (eq. 1.35):

$$\epsilon = -\frac{\dot{H}}{H^2} << 1 \rightarrow \ a(\tau) \approx -\frac{1}{H\tau}\frac{1}{1-\epsilon} \qquad \text{(at leading order in } \epsilon) \tag{3.8}$$

we can differentiate it with respect to conformal time to evaluate the time-dependent effective mass term a''/a appearing in the Mukhanov-Sasaki equation:

$$\frac{a''}{a} \approx \frac{2}{\tau^2}\,. \tag{3.9}$$

Substituting this potential into eq. 3.5, we obtain a differential equation that we can solve analytically:

$$v_k'' + \left(k^2 - \frac{2}{\tau^2}\right) v_k = 0\,. \tag{3.10}$$

The general solution to this equation can be expressed as a linear combination of Hankel functions of the first and second kind [4, 9]:

$$v_k(\tau) = A_k e^{-ik\tau}\left(1 + \frac{1}{ik\tau}\right) + B_k e^{ik\tau}\left(1 - \frac{1}{ik\tau}\right)\,. \tag{3.11}$$

To determine the mode amplitudes A_k and B_k, we must impose appropriate physical boundary conditions.

3.3.1 The Bunch-Davies vacuum

The choice of the integration constants is dictated by the selection of a vacuum state, necessity imposed by the time-dependence of the scale factor, as mentioned in sec 3.2. For each Fourier

mode, we select its natural ground state in the *ultraviolet limit*, where the physical wavelength of the mode is much smaller than the Hubble radius:

$$k^2 \gg \frac{a''}{a} \approx \frac{2}{\tau^2} \quad \Longrightarrow \quad |k\tau| \gg 1\,. \tag{3.12}$$

In this regime, the curvature of spacetime becomes negligible and the expansion is dynamically irrelevant, since the mode is deep inside the Hubble horizon; consequently, the mode function must behave as a standard plane wave with positive frequency in Minkowski space [4, 5]:

$$\lim_{k\tau\to-\infty} v_k(\tau) = \frac{1}{\sqrt{2k}} e^{-ik\tau}\,. \tag{3.13}$$

Imposing this asymptotic behavior fixes the constants to $A_k = 1$ and $B_k = 0$, which corresponds to choosing the **Bunch-Davies vacuum** and corresponds to the requirement that, in the ultraviolet (sub-horizon) limit, the FLRW spacetime is asymptotically Minkowskian. Imposing this vacuum choice yields the exact solution for the mode function (valid for all times) [4, 12]:

$$v_k(\tau) = \frac{e^{-ik\tau}}{\sqrt{2k}} \left(1 - \frac{i}{k\tau}\right)\,. \tag{3.14}$$

3.3.2 Horizon exit and mode freezing

The behaviour of the tensor modes described by the Muchanov equation exhibits two regimes, depending on the ratio of the wavelength to the Hubble radius:

1. **Sub-horizon limit ($|k\tau| \gg 1$):** As enforced by our boundary condition, deep inside the horizon the term k^2 dominates over the effective mass a''/a, so that the modes oscillate with decaying amplitude $h_k \sim v_k/a \propto 1/a$.

2. **Super-horizon limit ($|k\tau| \ll 1$):** As the Universe expands, the comoving Hubble radius $(aH)^{-1}$ shrinks, and eventually the mode exits the horizon. In this *infrared limit*, the interaction with the background geometry becomes dominant:

   $$v_k(\tau) \xrightarrow{|k\tau|\to 0} \frac{e^{-ik\tau}}{\sqrt{2k}} \left(-\frac{i}{k\tau}\right) \approx \frac{-i}{\sqrt{2}k^{3/2}\tau}\,. \tag{3.15}$$

   Since the physical tensor perturbation is related to the canonical variable by $h_k = \frac{2}{aM_{Pl}} v_k$, we find that the super-horizon amplitude of the gravitational wave approaches

a constant value [4, 9]:

$$|h_k| \propto \frac{1}{a}\left|\frac{1}{\tau}\right| \approx H \cdot \text{const}\,. \tag{3.16}$$

The latter phenomenon, where the evolution of the modes effectively stops as soon as they cross the horizon ($k = \frac{aH}{c}$), is known as **freeze-out**, or mode freezing.

3.3.3 Power spectrum of primordial tensor modes

We can finally apply the quantization procedure established in the previous section to the specific case of an inflationary background to derive the statistics of the field $v_{\mathbf{k}}$. As outlined before (eq. 3.7), although the expectation value of the field operator in the vacuum state is zero, $\langle 0|\hat{v}_{\mathbf{k}}|0\rangle = 0$, its variance is non-zero due to quantum fluctuations [4, 9]:

$$\langle 0|\hat{v}_{\mathbf{k}}(\tau)\hat{v}^{\dagger}_{\mathbf{k}'}(\tau)|0\rangle = (2\pi)^3\delta^{(3)}(\mathbf{k}-\mathbf{k}')|v_k(\tau)|^2\,. \tag{3.17}$$

From this variance, we can extract the dimensionless tensor power spectrum $\mathcal{P}_T(k)$ for the operator $\hat{h}_{ij}$; using 3.4 and summing over the two polarization states, the spectrum is defined as [4, 9]:

$$\mathcal{P}_T(k) = 2 \times \frac{4}{a^2 M_{Pl}^2}\frac{k^3}{2\pi^2}|v_k(\tau)|^2\,. \tag{3.18}$$

To compute this spectrum, we must consider the evolution of the modes relative to the Hubble horizon, as discussed in Sec. 3.3.2. In order to match the sub-horizon quantum fluctuations to the constant super-horizon solution, the perturbations are evaluated at the epoch of *horizon crossing*, defined by the condition $k = aH(\tau)$ [4, 6].

Substituting the mode function solution at horizon crossing $|v_k| \approx 1/\sqrt{2k}$ into Eq. 3.18, we obtain the well known result for the primordial tensor power spectrum [4, 9]:

$$\mathcal{P}_T(k) = \frac{2}{\pi^2}\left(\frac{H}{M_{Pl}}\right)^2\Bigg|_{k=aH}\,. \tag{3.19}$$

This key result directly links Quantum Mechanics (the amplitude of the gravitational waves is determined by H^2, arising from fluctuations) to General Relativity (the scale of gravity M_{Pl}^2).

It is important to note that the power spectrum depends on time τ but not on the spatial coordinates, reflecting the fact that the background is spatially homogeneous but evolves in time, and is *nearly* scale-invariant.

This deviation from exact scale invariance arises because different Fourier modes k exit the horizon at different times: Since the Hubble parameter H slowly decreases during inflation ($\dot{H} < 0$), modes with smaller k (which exit the horizon earlier) experience a larger H compared to modes with larger k (which exit later).

3.3.4 Tensor tilt

The deviation from exact scale invariance is quantified by the tensor spectral index, or *tensor tilt*, n_T:

$$n_T \equiv \frac{d \ln \mathcal{P}_T(k)}{d \ln k} \,. \tag{3.20}$$

Using the relation $d \ln k \approx d \ln a$ (valid at horizon crossing), we can express the tilt in terms of the slow-roll parameters$\epsilon = -\dot{H}/H^2$, we find [5, 4, 9]:

$$n_T = 2\frac{\dot{H}}{H^2} = -2\epsilon \,. \tag{3.21}$$

Since the condition for inflation requires $\epsilon > 0$, single-field slow-roll inflation inevitably predicts a negative tilt ($n_T < 0$): this corresponds to a *red-tilted* spectrum, where the amplitude decreases at higher frequencies. As noted in [16], the spectrum of a massless field in a quasi-de Sitter background behaves as $k^{-2\epsilon}$, confirming the red-tilt prediction.

However, slow-roll inflation is not necessarily described by a simple power law with a fixed spectral index. We could have a "running" index (changing spectral index with frequency). This is described as "slow-roll at Next-to-Leading Order" [17, 18].

3.3.5 Scalar perturbations and consistency relation

The computation of the scalar spectrum proceeds in a manner very similar to the tensor case, whereas the gauge-invariant quantity that describes scalar perturbations is the comoving curvature perturbation $\mathcal{R}$. The dimensionless power spectrum for scalar curvature perturbations is given by [10, 6, 9]:

$$\mathcal{P}_{\mathcal{R}}(k) = \frac{1}{8\pi^2}\frac{1}{\epsilon}\left(\frac{H}{M_{Pl}}\right)^2\Bigg|_{k=aH} \,. \tag{3.22}$$

Like tensor modes, scalar fluctuations also exhibit a nearly scale-invariant power spectrum, with a spectral index $n_s - 1 \approx 2\tau - 6\epsilon$.

The crucial difference lies in the dependence on the slow-roll parameter ϵ in the denominator of Eq. 3.22, which makes this power spectrum dependent on the specific inflationary model.

An important parameter to characterize the stochastic background is the *tensor-to-scalar ratio* r, defined as the ratio between the amplitude of the two power spectra at a pivot scale k_*:

$$r \equiv \frac{\mathcal{P}_T(k_*)}{\mathcal{P}_\mathcal{R}(k_*)} \,. \tag{3.23}$$

Substituting Eqs. 3.19, (Eq. 3.21) and 3.22, we obtain:

$$r = 16\epsilon = -8n_T \,. \tag{3.24}$$

This direct relation between the observable quantity r and n_T implies that a detection of the tensor amplitude, which would determine the tensor-to-scalar ratio, uniquely fixes the spectral slope n_T. Eq. 3.24 is known as the *consistency relation* for single-field slow-roll inflation [6, 9].

3.4 Post-inflationary evolution and the stochastic background

In the previous sections, we derived the primordial power spectrum of tensor perturbations, $\mathcal{P}_T(k)$, evaluated at the time of horizon exit during inflation. To connect this primordial prediction to present-day observables , we must track the evolution of tensor modes as they re-enter the horizon and propagate through the subsequent cosmological eras.

3.4.1 Horizon re-entry and the quantum-to-classical transition

Summarizing what we derived in 3.3.2, we saw that during the quasi-de Sitter expansion of inflation comoving scales k progressively exit the Hubble radius ($k \ll aH$) and freeze out, conserving their amplitude. After inflation ends, the comoving Hubble radius $(aH)^{-1}$ increases and modes that were frozen on super-horizon scales eventually re-enter the causal horizon when the condition $k = aH(\tau)$ is satisfied [4, 6].

Upon re-entry, the tensor modes, while generated as quantum vacuum fluctuations, are treated as classical stochastic fields of gravitational waves. This phenomenon, called *quantum squeezing*, renders the system effectively classical since, as shown by Baumann [4] and Figueroa [9], in the super-horizon limit ($k\tau \to 0$) the uncertainty in the field amplitude becomes negligible compared to the uncertainty in its conjugate momentum.

3.4.2 Evolution of tensor modes

The evolution of a tensor mode $h_k(\tau)$ after inflation is governed by the linearized Einstein equations in an expanding FLRW background. In the absence of anisotropic stress sources, and ignoring the damping due to free-streaming neutrinos, the equation of motion is [5, 9, 19, 20]:

$$h_k''(\tau) + 2\mathcal{H}(\tau)h_k'(\tau) + c^2k^2h_k(\tau) = 0\,. \tag{3.25}$$

The behavior of the solution depends critically on the background equation of state w at the time of re-entry.

Radiation Domination (RD): For modes entering the horizon during the radiation-dominated era (which includes all frequencies accessible to interferometers such as LIGO, Virgo, and LISA), the scale factor evolves as $a(\tau) \propto \tau$. The exact solution to Eq. 3.25 is given by [5]:

$$h_k(\tau) = h_k^{\rm prim}\,\frac{\sin(k\tau)}{k\tau}\,. \tag{3.26}$$

Deep inside the horizon ($k\tau \gg 1$), this solution describes a damped oscillation $h_k \propto a^{-1}e^{\pm ik\tau}$, whose amplitude decays as $1/\tau$

Matter Domination (MD): The general solution for perturbations that enter during matter domination ($a \propto \tau^2$) is a linear combination of constant and decaying modes. **Λ-Domination:** Modes re-entering during the dark-energy (Λ) dominated era follow a different evolution; however, as these scales are of the order of the current Hubble radius ($k \sim H_0$), they lie far below the frequency band of direct gravitational wave detectors [5].

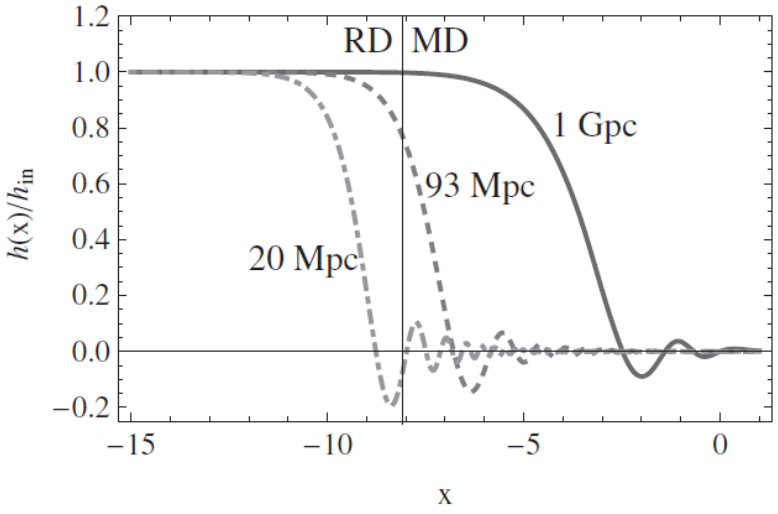


Figure 3.1: Evolution of the normalized gravitational wave amplitude $h_k(\tau)/h_{in}$against the logarithm of the scale factor $x = ln(a)$. The selected reduced wavelengths correspond to modes entering the horizon during the radiation-dominated era (20 Mpc), at the epoch of equality (93 Mpc), and during the matter-dominated era (1 Gpc). The figure highlights the universal $a^{-}1$ damping of the tensor modes once they cross the Hubble radius. Adapted from [5]

.

3.4.3 The transfer function

To encapsulate the evolution of the mode through different cosmological epochs (inflation → RD → MD), it is convenient to introduce a **Transfer Function** $T(k)$. This function maps the primordial amplitude set by inflation to the value of the field at late times τ_0 [9, 6]:

$$h_k(\tau_0) = h_k^{\text{prim}} \cdot T(k, \tau_0)\,. \tag{3.27}$$

The transfer function accounts for the damping due to cosmic expansion and the transitions between different equations of state. An approximate analytical form for modes entering during RD is given by [5]:

$$T(k, \tau_0) \approx \frac{3j_1(k\tau_0)}{k\tau_0}. \tag{3.28}$$

where $j_1(k\tau_0)$ is a spherical Bessel function. Eq 3.28 captures the transition from the scale-invariant behaviour at super-horizon scales to the oscillatory decay at sub-horizon scales.

3.4.4 Present-Day energy density spectrum

Experimental searches for the Stochastic Gravitational Wave Background (SGWB) do not measure the metric perturbation h_{ij} directly, but rather its spectral energy density. The strength of the SGWB is characterized by the dimensionless energy density parameter $\Omega_{GW}(f)$ [9]:

$$\Omega_{GW}(f) \equiv \frac{1}{\rho_{c,0}} \frac{d\rho_{GW}}{d\ln f}\,, \tag{3.29}$$

where $\rho_{c,0} = 3H_0^2/8\pi G$ is the critical density today and $f = k/2\pi$. Using the relation $\rho_{GW} \propto \langle \dot{h}_{ij}\dot{h}^{ij} \rangle$ and averaging over oscillations, the observable spectrum is related to the primordial tensor power spectrum $\mathcal{P}_T(k)$ (eq. 3.19) by [6, 9]:

$$\Omega_{GW}(f) = \frac{\Omega_{r,0}}{24}\mathcal{P}_T(f) \left(\frac{g_*(f)}{g_{*0}}\right) \left(\frac{g_{*S}(f)}{g_{*S0}}\right)^{-4/3} \mathcal{T}^2(f)\,. \tag{3.30}$$

Here, $\Omega_{r,0}h^2$ represents the radiation density parameter today, and the terms g_* and g_{*S} are the effective degrees of freedom for energy and entropy density.

For the standard single-field slow-roll inflation, where $\mathcal{P}_T(k)$ is nearly scale-invariant, eq. 3.30 predicts a characteristic shape for the SGWB:

1. **High Frequencies (Interferometers):** For modes that re-entered during Radiation Domination ($f \gg f_{eq} \sim 10^{-16}$ Hz), the transfer function is constant. The spectrum is a flat plateau, $\Omega_{GW} \sim$ const, determined solely by the inflationary energy scale H^2/M_{Pl}^2.

2. **Low Frequencies (CMB/PTA):** For modes entering during Matter Domination, the transfer function imposes a slope $\Omega_{GW}(f) \propto f^{-2}$.

3.5 Beyond slow-roll: blue-tilted spectra from non-standard Scenarios

The standard single-field slow-roll scenario (SFSR) discussed in the previous sections predicts a nearly scale-invariant, red tilted ($n_T \approx -2\epsilon < 0$) spectrum for tensor perturbations; while this prediction is consistent with current CMB constraints, it implies that the signal from a primordial gravitational wave background would fall below the sensitivity curve of direct detection experiments (such as Pulsar Timing Arrays, LISA, and LIGO/Virgo/KAGRA).

Therefore, a potential detection would require a scenario where the standard consistency relation that characterizes slow-roll is violated, leading to a blue-tilted spectrum. We now turn to briefly inquire about some of the exotic mechanisms beyond slow-roll inflation that could produce GW amplitudes detectable by modern interferometers.

3.5.1 Axion inflation and gauge field coupling

One of the most promising mechanisms for enhancing gravitational waves at small scales involves the presence of "axion-like" particles. In these models, due to its pseudo-scalar nature, the inflaton can couple to gauge fields through a parity-violating interaction term of the form [1] [9, 21]:

$$\mathcal{L}_{int} \propto -\frac{\phi}{4f} F_{\mu\nu}\tilde{F}^{\mu\nu}\,, \tag{3.31}$$

where $F_{\mu\nu}$ is the field strength tensor, $\tilde{F}^{\mu\nu}$ its dual, and f the axion decay constant. As the axion rolls down its potential, this coupling acts as a source of exponential production of gauge bosons, which in turn source tensor perturbations via their anisotropic stress. This source term is scale-dependent and typically grows towards the end of inflation, resulting in a strongly blue-tilted tensor spectrum ($n_T \approx 2$ in some regimes) [9], which carries two distinctive signatures that distinguish it from vacuum fluctuations:

- **Chirality:** Since the interaction in Eq. (3.31) violates parity, only one polarization state of the gravitational wave is exponentially enhanced.[22, 23]
- **Non-Gaussianity:** The signal originates from non-linear source terms, leading to highly non-Gaussian statistics.

3.5.2 Spectator fields with low sound speed

A blue tilt can also be generated by a scalar "spectator" field σ that is present during inflation, but does not drive the expansion. If this field has a small sound speed $c_s \ll 1$, its vacuum fluctuations are amplified, and the spatial gradients of these perturbations ($\partial_i\sigma\partial_j\sigma$) act as a

[1] In this section, we adopt natural units $\hbar = c = 1$ to follow standard particle physics notation

second-order source for gravitational waves [9]. While this mechanism can produce blue spectra, it faces severe observational constraints, since the enhancement affecting tensor modes scales reflects even more heavily on scalar density perturbations ($\mathcal{P}_{\mathcal{R}} \propto c_s^{-7}$ vs $\mathcal{P}_T \propto c_s^{-3}$). This makes this scenario less promising than the axion case, considering that the production of detectable GWs often implies overproducing scalar perturbations beyond the CMB limits [9].

3.5.3 Effective Field Theory (EFT) and Modified Gravity

We can also analyze inflation using the Effective Field Theory (EFT) approach, without specifying the exact potential driving the expansion and focusing the description on symmetry breaking. In this framework, inflation is described by the breaking of time-diffeomorphisms. In addition, one could consider scenarios that also break *spatial* diffeomorphisms (such as the Solid Inflation model), which could result in outcomes that go beyond General Relativity: [6, 9].

- **Massive Graviton:** If the graviton acquires a time-dependent mass $m_h(t)$ during inflation, the evolution of the mode function is altered. If $m_h^2 > 0$, the super-horizon modes are not frozen but can grow, leading to a blue tilt $n_T \approx \frac{2}{3}\frac{m_h^2}{H^2}$ [9].

- **Varying Sound Speed:** Alternatively, in EFT models where the propagation speed of tensor modes $c_T(t)$ deviates from the speed of light, the spectral index acquires a correction:

$$n_T = -2\epsilon - \epsilon_{c_T}\,, \quad \text{with} \quad \epsilon_{c_T} = \frac{\dot{c}_T}{H c_T}\,. \tag{3.32}$$

  If the speed of gravity decreases sufficiently fast during inflation ($\dot{c}_T < 0$), the term $-\epsilon_{c_T}$ becomes positive and dominant, yielding a blue spectrum [6].

3.5.4 Post-inflationary enhancement: the stiff era

Finally, a blue spectrum observed today does not necessarily imply a blue spectrum at production, given that the transfer function $T(k)$ depends on the expansion history of the Universe.

Up until now, we considered the standard cosmological scenario, where the Universe enters a radiation-dominated phase immediately after inflation. However, if there is an intermediate

"stiff" era dominated by the kinetic energy of the inflaton (kination), with an equation of state of $w > 1/3$, the background energy density $\rho_{bkg} \propto a^{-3(1+w)}$ would decay faster than the radiation-like energy density of gravitational waves ($\rho_{GW} \propto a^{-4}$). This would result in the relative amplification of high-frequency modes (which re-enter the horizon earlier), and in an observed spectral tilt n_T^{obs} related to the primordial tilt n_T^{prim} by [9, 5]:

$$n_T^{obs} = n_T^{prim} + \frac{6w-2}{3w+1}\,. \tag{3.33}$$

For a stiff fluid with $w = 1$, this induces a strong blue tilt ($n_T^{obs} \approx 1$) on the high-frequency tail of the spectrum, potentially bringing the signal within the reach of laser interferometers.

3.6 Beyond linear order: scalar induced gravitational waves

Up to this point, our analysis has relied on the first-order approximation of cosmological perturbation theory. In this linear regime, scalar perturbations (density fluctuations) and tensor perturbations (gravitational waves) evolve independently. However, General Relativity is an inherently non-linear theory, thus it is only natural to consider extending our analysis to *second order* in perturbation theory. We will find that in this context scalar perturbations act as a source for tensor modes, generating a secondary background of **Scalar Induced Gravitational Waves (SIGWs)**[24, 25]. While this effect is negligible for the standard nearly scale-invariant spectrum observed at CMB scales ($\mathcal{P}_\mathcal{R} \sim 10^{-9}$), it becomes significant if the primordial scalar power spectrum is strongly enhanced ($\mathcal{P}_\mathcal{R} \sim 10^{-2}$) on small scales/high frequencies.

3.6.1 Second-order Einstein equations and the source term

To describe this phenomenon mathematically, we consider the perturbed Friedmann-Lemaître-Robertson-Walker metric, this time including second-order tensor perturbations $h_{ij}^{(2)}$, so that the line element is given by [9, 12]:

$$ds^2 = a^2(\tau)\left[-(1+2\Phi)d\tau^2 + \left((1-2\Psi)\delta_{ij} + \frac{1}{2}h_{ij}^{(2)}\right)dx^i dx^j\right]\,, \tag{3.34}$$

where Φ and Ψ are the first-order scalar Bardeen potentials, which become $\Phi = \Psi$ in the absence of anisotropic stress at first order.

Substituting this metric into the Einstein field equations and expanding to second order, one finds that the equation of motion for the tensor modes is no longer homogeneous, and takes the form of a wave equation with a source term S_{ij} [9, 6]:

$$h''_{ij}(\mathbf{k},\tau) + 2\mathcal{H}h'_{ij}(\mathbf{k},\tau) + k^2 h_{ij}(\mathbf{k},\tau) = 4S^{TT}_{ij}(\mathbf{k},\tau)\,. \tag{3.35}$$

The term S_{ij} arises purely from the scalar metric perturbations, and in real space represents the anisotropic stress induced by scalar field gradients [9]:

$$S_{ij} \propto \partial_i\Phi\partial_j\Phi - \frac{1}{3}\delta_{ij}(\partial_k\Phi)^2\,. \tag{3.36}$$

Physically, this implies that the interaction of two first-order scalar modes acts as a source for a second-order tensor mode. This production mechanism is particularly efficient when the scalar modes re-enter the cosmological horizon during the radiation-dominated era, since in this phase the gravitational potential Φ oscillates and decays, generating a resonating quadrupole moment that leads to a significant amplification of the gravitational wave amplitude [4, 9].

3.6.2 Power spectrum and features

To derive the observable spectrum of SIGWs, we relate the source term to the primordial scalar power spectrum found in Eq.3.22: assuming that the scalar perturbations obey Gaussian statistics and neglecting the anisotropic stress due to neutrinos, the spectral density of induced gravitational waves today can be expressed as [9, 25, 6]:

$$\Omega^{(SIGW)}_{GW}(k) \propto \left(\mathcal{P}_{\mathcal{R}}(k)\right)^2\,. \tag{3.37}$$

This quadratic dependence, $\Omega_{GW} \sim \langle h^2\rangle \sim \langle S^2\rangle \sim \langle\Phi^4\rangle$, suggest profound differences that distinguish SIGWs from the standard inflationary vacuum fluctuations[24]:

1. **Violation of Scale Invariance:** Unlike the first-order tensor spectrum derived in Section 3.4, which is nearly scale-invariant ($n_T \approx 0$), the SIGW spectrum is highly sensitive to the shape of the scalar spectrum. If $\mathcal{P}_{\mathcal{R}}(k)$ exhibits a peak at a specific scale k_*, the induced GW spectrum will exhibit a corresponding peak at $f \approx ck_*/2\pi$ [9].

2. **Connection to Primordial Black Holes (PBHs):** A truly interesting aspect of SIGWs is their relation to Primordial Black Holes. PBHs can form if the primordial density perturbations are extremely large ($\delta\rho/\rho \sim 1$) upon horizon re-entry, which requires the primordial scalar power spectrum to be enhanced by orders of magnitude ($\mathcal{P}_\mathcal{R} \sim 10^{-2}$) compared to the amplitude observed at CMB scales ($\mathcal{P}_\mathcal{R} \sim 10^{-9}$) [9, 26]. Such a large increase inevitably generates a detectable background of induced gravitational waves.

3. **Insight on the "Dark Ages" of Inflation:** The detection of SIGWs would allow us to probe the physics of inflation at small scales that are completely inaccessible to CMB observations. While the CMB constrains the universe on scales $k \sim 0.002 - 0.2\,\mathrm{Mpc}^{-1}$, interferometers like LISA and Einstein Telescope probe scales $k \sim 10^{12} - 10^{16}\,\mathrm{Mpc}^{-1}$ [6, 9]; therefore, observing a SIGW signal would provide a unique window into the dynamics of the inflaton field (e.g., features in the potential) towards the end of inflation.

3.6.3 Alternative cosmological mechanisms of GW production

Beyond the irreducible background from inflation (Section 3.2) and the induced second-order waves (Section 3.4), the early Universe may have hosted high-energy non-equilibrium processes capable of generating distinct stochastic GW backgrounds. We briefly summarize three main examples of such mechanisms.

Preheating and Parametric Resonance

The transition from the cold, low-entropy state of inflation to the hot, thermalized plasma of the Big Bang is known as reheating. In many inflationary models, the initial stage of this energy transfer—termed *preheating*—occurs via non-perturbative effects, such as parametric resonance [5, 4]. During this phase, the inflaton field ϕ oscillates rapidly around the minimum of its potential, inducing an explosive production of particles coupled to it; this process generates large, time-dependent inhomogeneities in the energy-momentum tensor which act as a powerful source of gravitational waves [9]. Unlike the scale-invariant spectrum of slow-roll inflation, the GW spectrum from preheating is typically peaked at very high frequencies determined by the energy scale of inflation. For models ending at the Grand Unified Theory (GUT) scale, these frequencies lie in the MHz-GHz range [5, 9].

First-Order Phase Transitions

As the Universe expands and cools, it undergoes symmetry-breaking phase transitions (e.g., electroweak, QCD). If a transition is of *first order*, it proceeds through the nucleation of bubbles of the stable "true vacuum" phase within the metastable "false vacuum" background [5, 4]. This process is governed by quantum tunneling across the potential barrier separating the two phases. The nucleated bubbles expand rapidly due to the pressure differential, eventually colliding and merging, releasing energy; part of it is transferred to coupled fields generating an anisotropic stress component of the fluid energy momentum tensor: this can act as a source of gw [9, 6]:

The resulting spectrum is generally a broken power law, with a peak frequency linked to the temperature of the Universe at the time of the transition (T_*). For phase transitions occurring at the electroweak scale ($T_* \sim 100$ GeV), the peak falls in the mHz range, making it a prime target for the LISA mission [27, 28].

Cosmic Strings

Phase transitions can also leave behind one-dimensional topological defects, known as *cosmic strings* [29, 5, 9]. These strings form a complex evolving network, and intersect creating loops that oscillate at relativistic speeds; when these loops decay, they do so primarily by emitting gravitational radiation. Because strings are continuously produced - and thus decay- throughout the history of the universe, they generate a stochastic background of GWs having a nearly scale-invariant (flat) spectrum, spanning range of frequencies from the nanohertz (probed by Pulsar Timing Arrays) up to the kilohertz range (LIGO/Virgo) [9, 30].

Chapter 4

OBSERVATIONAL PERSPECTIVES ON STOCHASTIC GRAVITATIONAL-WAVE BACKGROUNDS

In the previous chapters, we described the mechanisms responsible for the production of primordial gravitational waves and their evolution; we determined the tensor power spectrum $\mathcal{P}_t(k)$ and the present-day spectral energy density $\Omega_{\rm GW}(f)$ which encode decisive information about high-energy physics and the dynamics of the early Universe.

We now turn to confront these theoretical predictions with observational reality, exploring the experimental prospects for detecting a relic gravitational-wave background generated during inflation. As anticipated, the identification of such a signal would provide direct insight into early-Universe physics and energy scales far beyond the reach of terrestrial experiments.

If present, the inflationary background is expected to be extremely weak and challenging to detect with current instruments; nevertheless, several ongoing and future projects are specifically designed to probe stochastic gravitational-wave backgrounds across different frequency bands.

In the following sections, we review current gravitational-wave observations, some suggested future searches, discuss recent results from Pulsar Timing Arrays, and examine how the non-detection of primordial tensor modes in the polarization of the Cosmic Microwave Background places stringent constraints on inflationary models.

4.1 Gravitational wave detection

As briefly mentioned in the historical overview of Chapter 1, the first direct detection of gravitational waves occurred in 2015, approximately one century after their theoretical prediction within General Relativity.Following the initial decades of debate over their existence -which was questioned by Einstein himself at certain stages- the experimental search eventually began in the 1960s with the pioneering work of Joseph Weber, who claimed evidence of gravitational-wave signals using resonant-mass detectors (the so-called Weber bars). Although these results were never independently confirmed, his work managed to spark scientific interest in the possibility of measuring gravitational radiation. [31].

During the same period, several researchers (including Gertsenshtein, Pustovoit, Weiss, Forward, and Drever) developed, in parallel but independently, the idea of detecting gravitational waves using laser interferometry. This approach proved particularly promising, since kilometer-scale interferometers could in principle achieve the strain sensitivity required to probe astrophysical sources. [10].

4.1.1 Interferometric principle

Modern ground-based detectors operate according to the Michelson interferometer configuration: a monochromatic laser beam is split by a beam splitter into two perpendicular arms; the beams are then reflected by mirrors and recombined at the photodetector. In the absence of gravitational waves, the optical paths are adjusted to produce destructive interference at the output port. As discussed in Chapter 2.2, a passing gravitational wave produces a quadrupolar distortion of spacetime, causing an alternating stretching and squeezing of orthogonal spatial directions. The dimensionless strain amplitude is defined as

$$h \equiv \frac{\Delta L}{L}, \tag{4.1}$$

where L is the arm length of the interferometer and ΔL is the differential change induced by the wave. In the interferometer, the arm length distortion induces a differential phase shift between the two arms, resulting in a measurable variation in the interference pattern.

Typical astrophysical signals reaching Earth correspond to strains of order $h \sim 10^{-21}$, making their detection extremely difficult.

4.1.2 Gravitational wave detectors

Ground-Based Detectors

The first interferometric prototype was constructed by Robert Forward in 1971, although large-scale kilometer interferometers were realized only in the 1990s and early 2000s. Major facilities include LIGO in the United States, Virgo in Italy, and GEO600 in Germany, later joined by KAGRA in Japan.

Second-generation detectors such as Advanced LIGO and Advanced Virgo implement several technological improvements beyond the simple Michelson design, including seismic isolation systems to reduce ground vibrations, Fabry–Pérot cavities within the arms to increase the effective optical path length, and power-recycling techniques to enhance laser power and reduce quantum noise. These instruments are primarily sensitive to high-frequency gravitational waves in the range $\sim 10\,\mathrm{Hz}$ to $\sim 10\,\mathrm{kHz}$, targeting compact binary mergers involving stellar-mass black holes and neutron stars.

Future third-generation observatories, such as the Einstein Telescope (ET), aim to further improve sensitivity by roughly one order of magnitude and extend the low-frequency reach down to $\sim 1\,\mathrm{Hz}$ through underground installation and cryogenic technologies.

Space-based detectors

To reach lower frequencies that are inaccessible from the ground due to seismic and Newtonian noise, space-based interferometers are required. The Laser Interferometer Space Antenna (LISA), planned as a mission of the European Space Agency, is expected to operate in the frequency band 10^{-4}–$10^{-1}\,\mathrm{Hz}$.

LISA will consist of three spacecraft arranged in an approximately equilateral triangle with arm lengths of about $2.5 \times 10^{6}\,\mathrm{km}$, following a heliocentric orbit behind Earth. Its sensitivity will allow for the detection of gravitational waves from supermassive black hole mergers, extreme mass-ratio inspirals, and possibly cosmological backgrounds at mHz frequencies.

Pulsar Timing Arrays

Ultra-low-frequency gravitational waves, in the nanohertz regime ($\sim 10^{-9}$–10^{-7} Hz), can be probed using the galaxy itself as a "detector". Millisecond pulsars (rapidly rotating, highly magnetized neutron stars that emit beams of electromagnetic radiation) can act as remarkably stable cosmic clocks: when the Earth lies within the beam, the observed pulses form an extremely regular signal, allowing the path between Earth and the pulsar to be treated as the arm of a cosmic gravitational wave detector.

By monitoring a network of such pulsars, known as a Pulsar Timing Array (PTA), over timescales of years to decades, one can search for the passage of gravitational waves by correlating the deviations in the pulse arrival times (timing residuals) across the sky.

The principal collaborations currently operating PTAs are the North American Nanohertz Observatory for Gravitational Waves (NANOGrav), the European Pulsar Timing Array (EPTA) in combination with the Indian Pulsar Timing Array (InPTA), the Parkes Pulsar Timing Array (PPTA), and the Chinese Pulsar Timing Array (CPTA); together they form the International Pulsar Timing Array (IPTA).

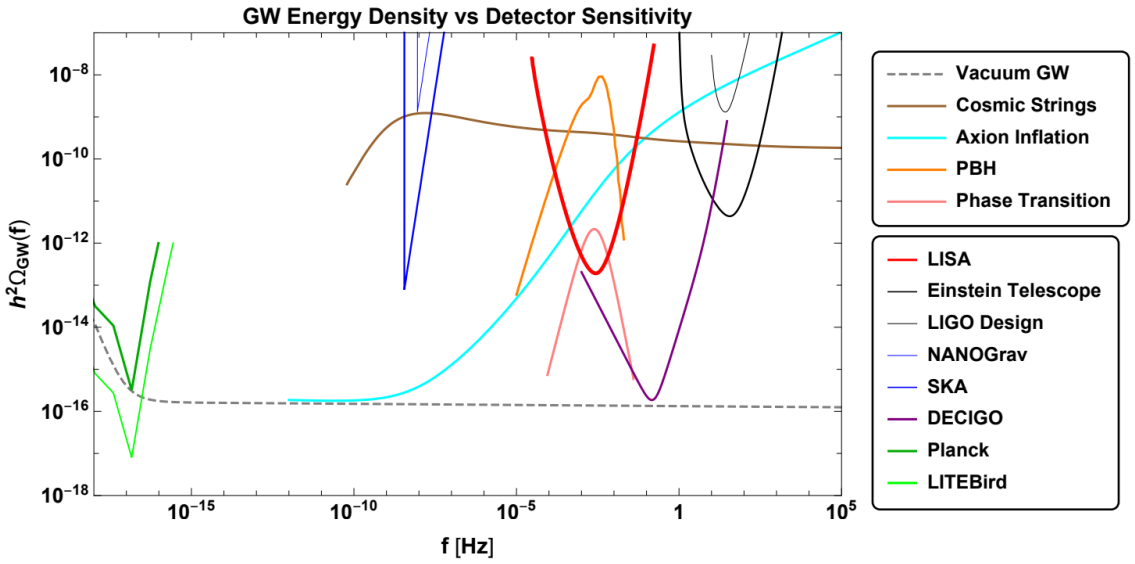


Figure 4.1: Comparison of the SGWB spectral energy density, $h^2\Omega_{\rm GW}$, predicted by various cosmological mechanisms (the grey dashed line labeled vacuum GW refers to standard slow-roll inflation vacuum fluctuations) against the sensitivity curves of current and future detectors. Credits:[32].

Table 4.1: Overview of frequency bands and target sources for GW detectors.

Band	**Frequencies**	**Detectors**	**Main sources**
Extremely Low	$\sim 10^{-18} - 10^{-16}$ Hz	**CMB** (B-Modes): Planck, BICEP/Keck, LiteBIRD	PGWs, Phase transitions
Ultra-Low	$\sim 10^{-9} - 10^{-7}$ Hz	**PTA**: NANOGrav, EPTA, InPTA, PPTA, CPTA, MeerKAT, SKA	SMBHBs, Phase transitions, Cosmic Strings
Low / Mid	$\sim 10^{-4} - 1$ Hz	**space-based**: LISA, DECIGO	Galactic binaries, MBH mergers, EMRI
High	$\sim 1 - 10^{4}$ Hz	**ground-based**: LIGO, Virgo, ET	Stellar BH and neutron star mergers

The different detection strategies described above are complementary, each probing distinct frequency bands and therefore different classes of gravitational-wave sources: ground-based interferometers are sensitive to high-frequency astrophysical events, space-based missions explore the millihertz regime, and PTAs provide access to the nanohertz window. This broad frequency coverage is essential for testing both astrophysical models and cosmological scenarios for the production of a stochastic gravitational-wave background.

4.2 Constraints on inflation models from the CMB

While direct gravitational wave detectors search for astrophysical and cosmological sources across a wide range of frequencies, the Cosmic Microwave Background (CMB) provides a snapshot of the Universe at the surface of last scattering (at redshift $z \approx 1100$), offering the strictest constraints on primordial gravitational waves (PGWs) at extremely large scales ($f \sim 10^{-17}$ Hz).[33]

Physics of the CMB: anisotropies and polarization

The Cosmic Microwave Background (CMB) is the fossil radiation released approximately 380,000 years after the Big Bang, when the Universe had cooled sufficiently to allow the formation of neutral hydrogen atoms: this process is known as recombination; at this moment, the Universe became transparent to radiation, allowing photons to stream freely [4, 6]. This radiation follows a blackbody spectrum with extraordinary precision at a current temperature of $T_0 \approx 2.725$ K [4, 1], as observed from the discovery by Penzias and Wilson in 1965, up to the satellite missions COBE, WMAP, and Planck.

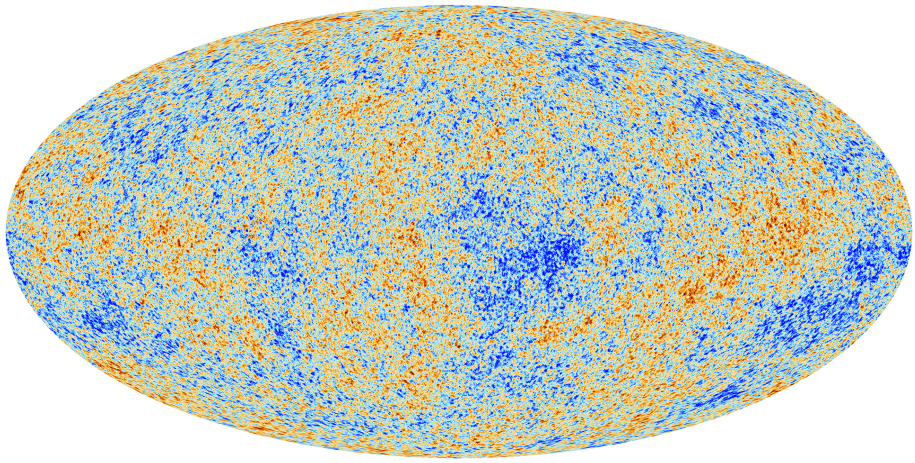


Figure 4.2: Full-sky map of the Cosmic Microwave Background (CMB) temperature anisotropies as measured by the Planck satellite. These tiny temperature fluctuations, on the order of $\Delta T/T \approx 10^{=5}$, directly reflect the primordial density perturbations of the photon-baryon fluid at the epoch of recombination. Credits:ESA / Planck Collaboration [33]

Although the CMB is extremely isotropic, it exhibits slight temperature fluctuations ($\Delta T/T \sim 10^{-5}$), which are the direct trace of primordial density perturbations that acted as seeds for the formation of cosmic structures [4, 2]. Beyond these anisotropies, the CMB radiation is also characterized by a polarization pattern generated by Thomson scattering of photons off of free electrons during recombination, when the primordial plasma possessed a local quadrupolar anisotropy [4, 6, 5].

The polarization field can be decomposed into two orthogonal modes based on their parity properties:

- **E-modes (Gradient-like components):** These are sourced by both scalar (density) and tensor (GW) perturbations, and have even parity.
- **B-modes (Curl-like components):** These exhibit a pattern with odd parity. Since in linear perturbation theory, scalar perturbations do not source B-modes, the detection of primordial B-modes would be a unique signature of tensor perturbations (PGWs) [34].

Limits on the tensor-to-scalar ratio

In chapter 3.3.5 we introduced the tensor to scalar ratio $r \equiv \mathcal{P}_T(k_*)/\mathcal{P}_\mathcal{R}(k_*)$ at a pivot scale k_*, to characterize the amplitude of tensor modes relative to scalar perturbations. We showed that the energy scale of inflation is determined by the tensor amplitude ($V^{1/4} \propto r^{1/4}$), since

$$\mathcal{P}_T(k) = \frac{2}{\pi^2}\left(\frac{H}{M_{\rm Pl}}\right)^2, \tag{4.2}$$

This means that constraining r directly determines the energy scale of inflation.

To date, no primordial B-modes have been detected from *Planck* and BICEP/Keck; nonetheless, we can combine these data to strongly disfavor many large field inflationary models such as monomial potentials $V(\phi) \propto \phi^p$ with $p \geq 2$, e.g. chaotic inflation with $m^2\phi^2$. Using data up to the latest observing season (BK2023 + Plank legacy), the strongest upper limit for r was found to be [31, 6]:

$$r_{0.05} < 0.032. \tag{4.3}$$

(at 95% confidence level, at the pivot scale $k = 0.05\,\mathrm{Mpc}^{-1}$)

This bound favors scenarios predicting smaller tensor amplitudes, such as plateau-like potentials (Starobinsky R^2 model or Higgs inflation, which predict $r \sim 0.003$) [35].

Future CMB polarization experiments, such as the ground-based CMB-S4 and the satellite mission LiteBIRD, aim to reach sensitivities of order $\sigma(r) \sim 10^{-3}$, potentially allowing for a detection if $r \gtrsim 10^{-3}$. A confirmed detection of primordial B-modes would not only establish the existence of inflationary gravitational waves, but would also provide solid evidence that gravity itself underwent quantum fluctuations in the early Universe: therefore, although no

primordial tensor signal has yet been observed in the CMB, current and forthcoming measurements remain the most exciting and promising pursuit for inflationary gravitational waves on the largest cosmological scales.

4.3 Background detection: recent results and implications

Stochastic gravitational wave background

In this dissertation, we investigated the existence of a Stochastic Gravitational Wave Background (SGWB) generated during inflation, leading to a nearly Gaussian distribution with a broad frequency spectrum.

When interpreting observational data, however, we cannot ignore that such a stochastic background could also be motivated by a different - yet equally compelling and significant - possibility, which has not been discussed in this work: an astrophysical origin.

Such a signal would arise from the superposition of a large number of individual, unresolved astrophysical sources, such as black hole binaries and neutron star mergers, among others. While containing valuable astrophysical information about galactic formation and evolution, from the cosmological perspective it would act as a foreground to model and subtract from our data; it is therefore essential to acknowledge this alternative when examining experimental observations.

PTA 2023: evidence for a background

In June 2023, major PTA collaborations (NANOGrav, EPTA, InPTA, PPTA, CPTA) announced historical results based on the collection and analysis of years of data, reporting independent evidence for a common-spectrum stochastic signal [36, 26]. These datasets show (with statistical significance ranging between 3σ and 4σ) spatial correlations among pulsars which are consistent with the Hellings–Downs curve [37]: this quadrupolar angular correlation pattern is the distinctive fingerprint of an isotropic stochastic gravitational-wave background within General Relativity, distinguishing it from monopolar or dipolar noise sources [26, 36].

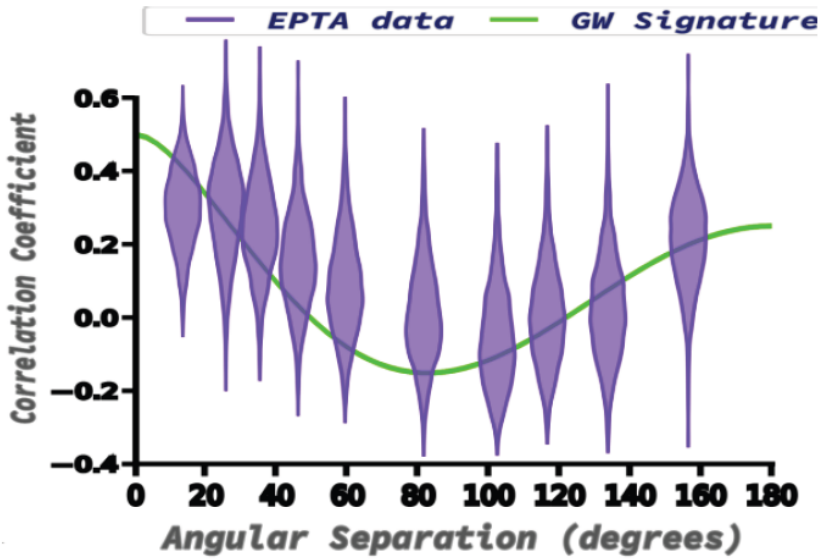


Figure 4.3: Measured spatial correlations between pulsar timing residuals as a function of their angular separation. The green solid line represents the theoretical Hellings-Downs expectation for an isotropic stochastic gravitational-wave background, while the violins show the posterior distributions of the measured correlation coefficients from the EPTA second data release. Figure adapted from [38]

The characteristic strain spectrum reported by PTAs is modeled as a power law:

$$h_c(f) = A_{\rm GWB} \left(\frac{f}{f_{\rm yr}} \right)^{\alpha}, \tag{4.4}$$

where $A_{\rm GWB}$ is the amplitude at a reference frequency of $f_{\rm yr} = 1\,{\rm yr}^{-1}$ and α determines the spectral slope. In the PTA literature, this is often related to the power spectral density (PSD) index $\gamma = 3 - 2\alpha$ [31]. The measured amplitude is of the order $A_{\rm GWB} \approx 2\text{–}3 \times 10^{-15}$ [26, 36].

- **Astrophysical Hypotheses** The leading astrophysical interpretation attributes this background to the cumulative emission from inspiraling supermassive black hole binaries (SMBHBs) formed during galaxy mergers. For a population of binaries driven solely by the gravitational wave emission in circular orbits, the spectral index is predicted to be $\alpha = -2/3$ (corresponding to $\gamma = 13/3 \approx 4.33$) [26, 39]. However, the 2023 analyses indicate a spectral slope that is slightly flatter than this standard prediction (with measured $\gamma \approx 3.2 - 3.8$ in some datasets) [36]. This deviation could imply the presence of envi-

ronmental effects (such as stellar hardening or interaction with gas) or high eccentricity in the binary population, but it also leaves room for cosmological interpretations.

- **Cosmological interpretation** From a cosmological perspective, the observed signal can be well-fitted by several "New Physics" scenarios. As discussed in Chapter 3, standard single-field slow-roll inflation predicts a red-tilted tensor spectrum ($n_T = -r/8$) with an amplitude $\Omega_{\rm GW}h^2 \lesssim 10^{-16}$, which is unobservable by PTAs today.

  To explain the high amplitude observed ($A_{\rm GWB} \sim 10^{-15}$), an inflationary origin requires a significant violation of the standard consistency relations, specifically a blue tilt ($n_T \approx 2$) in the tensor spectrum, implying non-standard inflationary dynamics, previously mentioned in 3.5.

  Other cosmological sources provide competitive fits to the data. These include:

  - **Cosmic Strings:** A network of stable cosmic strings is a viable candidate, although the data are in tension with upper limits from standard cosmological models unless the loop distribution is modified [30].
  - **Phase Transitions and Domain Walls:** First-order phase transitions occurring at temperatures $T_* \sim 100$ MeV or annihilating domain walls provide excellent fits to the spectral shape observed by NANOGrav and EPTA, potentially fitting the data better than the standard astrophysical model.
  - **Scalar-Induced GWs (SIGW):** The signal could arise from second-order GWs generated by enhanced primordial curvature perturbations. However, this scenario is tightly constrained because the required amplitude would often lead to an overproduction of Primordial Black Holes (PBHs), potentially exceeding the dark matter abundance unless significant non-Gaussianities are present [21].

Currently, the data cannot definitively distinguish between the astrophysical SMBHB baseline and these exotic cosmological origins; future observations with improved sensitivity and longer baselines will be necessary to discriminate between these sources.

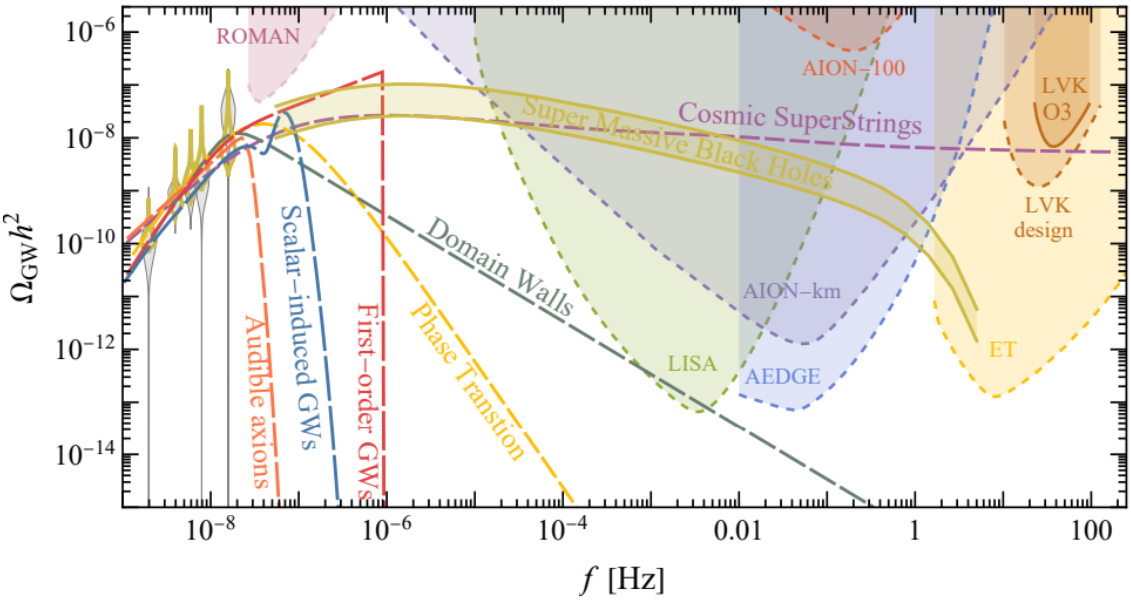


Figure 4.4: High-frequency extrapolation of the SGWB spectra derived from Pulsar Timing Array measurements, plotted against the sensitivity curves of present and future gravitational-wave detectors. The multi-band comparison demonstrates how future observatories will break the theoretical degeneracies: a cosmic string background would remain detectable across all higher-frequency bands, whereas signals from phase transitions or scalar perturbations face a high-frequency cut-off. Additionally, the standard astrophysical SMBHB background is expected to resolve into individually detectable binary mergers in the milli-Hertz and deci-Hertz regimes. Credits:[40].

In conclusion, while the stochastic background observed by PTAs is most naturally explained by supermassive black hole binaries, its precise characterization has profound implications for both astrophysics and early-Universe cosmology. Together with CMB constraints and direct interferometric searches, PTA observations complete a multi-frequency framework for probing gravitational-wave backgrounds across more than twenty orders of magnitude in frequency.

CONCLUSIONS

In this thesis, we have approached the topic of primordial gravitational waves and their crucial role in the cosmological study of the physics describing the birth of the Universe.

To understand how the analysis and possible detection of these cosmic messengers provide an unparalleled probe of the earliest stages of cosmic history, we began by introducing the foundations and main results of modern cosmology. It was then necessary to acquire the essential mathematical tools required to study the evolution of these physical degrees of freedom; we thus defined the formalism developed within General Relativity, describing the phenomenology and evolution of gravitational waves in a curved, expanding spacetime.

We then moved to the core of this work, namely the quantum production of tensor perturbations during the inflationary process. In particular, we explored in detail the standard single-field slow-roll inflationary scenario, while briefly addressing more complex alternative mechanisms and exotic models, together with their different predictions for the stochastic background they would generate. By exploiting the fundamental concepts of quantum mechanics and quantum field theory, we quantized the tensor modes in a quasi–de Sitter background, deriving the expression for the primordial power spectrum, and subsequently connecting it to the present-day spectral energy density through the transfer function.

We finally adopted an observational perspective, reviewing the current status of gravitational-wave detection and future prospects. We have seen that gravitational waves can be probed across a wide range of energy scales, through ground-based and space-based interferometers operating at high- and intermediate-frequency bands, as well as through Pulsar Timing Arrays acting as galactic-scale detectors in the ultra-low-frequency regime.

If one does not consider scenarios beyond minimal inflation, however, the most promising probe for directly accessing primordial tensor modes remains the search for B-mode polar-

ization in the Cosmic Microwave Background. Although such a detection has not yet been achieved, it represents one of the major challenges of contemporary cosmology, and current results already allow us to impose significant constraints on inflationary models, excluding several large-field potentials.

In recent years, evidence for a stochastic gravitational-wave background at nanohertz frequencies has been reported by major Pulsar Timing Arrays collaborations. Although the most conservative interpretation of this signal is astrophysical (attributing the signal to the cumulative emission from inspiraling SMBHBs) rather than cosmological, these results are nonetheless valuable for improving the characterization of the astrophysical background that will need to be modeled as a foreground (or effective noise) when isolating a primordial cosmological contribution.

If, on the other hand, a cosmological origin were to be confirmed, this would imply a radical revision of the minimal inflationary scenario and open the door to new physics in the embryonic Universe: specifically, since the standard single-field slow-roll paradigm predicts a red-tilted tensor spectrum ($n_T = = r/8$), the resulting energy density at interferometer and PTA scales would be vanishingly small ($\Omega_{GW} h^2 \approx 10^{=16}$). Consequently, the confirmed detection of a cosmological background in these frequency bands would necessitate a breakdown of the standard consistency relations, requiring mechanisms that produce a "blue" spectrum ($n_T > 0$) or distinctive spectral features. As we have discussed, such scenarios are theoretically well-motivated and include particle production by gauge fields during inflation, non-standard post-inflationary phases (such as a stiff-matter era or kination), or first-order phase transitions in the early Universe

In any case, we find ourselves at a turning point in gravitational-wave research. By exploiting the complementarity of different observational probes — CMB measurements, interferometric detectors, and Pulsar Timing Arrays — we are progressively increasing our ability to test General Relativity and quantum physics at energy scales approaching the Planck regime.

Although definitive observational results have not yet been reached, the rapid progress achieved in related fields gives reason for optimism within precision cosmology. Multi-messenger astronomy is continuously refining our theoretical predictions and models, and future missions together with technological improvements in detector sensitivity promise further ad-

vances in our understanding of primordial-Universe physics. Looking ahead, the future of primordial gravitational wave astronomy is extremely promising: while current constraints from the CMB and PTAs are already squeezing the parameter space of inflationary models, the next generation of experiments will be transformative. Future CMB missions, such as LiteBIRD and CMB-S4, aim to reach the sensitivity required to detect the imprint of standard slow-roll inflation or to lower the upper bound on the tensor-to-scalar ratio to $r \approx 10^{=3}$. Simultaneously, the upcoming space-based interferometer LISA, along with third-generation ground-based detectors like the Einstein Telescope and Cosmic Explorer, will open the milliHertz and deciHertz frequency windows. These instruments will not only possess the sensitivity to disentangle cosmological signals from astrophysical foregrounds through spectral shape reconstruction and anisotropy analysis, but will also bridge the gap between the low-frequency probes (PTA) and high-frequency observatories (LIGO/Virgo and Einstein Telescope).

Even in the absence of a breakthrough discovery such as the detection of primordial tensor modes — and thus direct evidence of quantum fluctuations of spacetime — it is profoundly exciting to recognize that we may be approaching a new era in which gravitational waves could finally provide the concrete link between quantum theory, gravity, and the physics of the very early Universe.

Bibliography

[1] Barbara Ryden. *Introduction to Cosmology*. Second. New York: Cambridge University Press, 2017. ISBN: 978-1-107-15483-4.

[2] Patrick Peter and Jean-Philippe Uzan. *Primordial Cosmology*. Oxford: Oxford University Press, 2009. ISBN: 978-0-19-920991-0.

[3] Éanna É. Flanagan and Scott A. Hughes. "The basics of gravitational wave theory". In: *New J. Phys.* 7 (2005), p. 204. DOI: 10.1088/1367-2630/7/1/204. arXiv: gr-qc/0501041.

[4] Daniel Baumann. *Cosmology*. Cambridge: Cambridge University Press, 2022. ISBN: 978-1-108-83807-8.

[5] Michele Maggiore. *Gravitational Waves. Vol. 2: Astrophysics and Cosmology*. Oxford: Oxford University Press, 2018. ISBN: 978-0-19-857089-9. DOI: 10.1093/oso/9780198570899.001.

[6] William Giarè. "Relics from the Early Universe: Primordial Gravitational Waves, Axions and Neutrinos". Doctoral Thesis. Sapienza University of Rome, 2021.

[7] Scott Dodelson. *Modern Cosmology*. Amsterdam: Academic Press, 2003. ISBN: 978-0-12-219141-1.

[8] Tamara M. Davis and Charles H. Lineweaver. "Expanding Confusion: common misconceptions of cosmological horizons and the superluminal expansion of the Universe". In: *Publ. Astron. Soc. Austral.* 21.1 (2004), pp. 97–109. DOI: 10.1071/AS03040. arXiv: astro-ph/0310808 [astro-ph].

[9] Chiara Caprini and Daniel G Figueroa. "Cosmological backgrounds of gravitational waves". In: *Classical and Quantum Gravity* 35.16 (2018), p. 163001. DOI: 10.1088/1361-6382/aac608.

[10] Michele Maggiore. *Gravitational Waves. Vol. 1: Theory and Experiments*. Oxford: Oxford University Press, 2008. ISBN: 978-0-19-857074-5.

[11] Michele Maggiore. "Gravitational wave experiments and early universe cosmology". In: *Physics Reports* 331.6 (2000), pp. 283–367. DOI: 10.1016/S0370-1573(99)00102-7.

[12] Nur Imanina Binti Mohd Faidzal. "Dissertation on Inflationary Paradigm". MA thesis. Imperial College London, 2017.

[13] A. A. Starobinsky. "Spectrum of relict gravitational radiation and the early state of the universe". In: *JETP Letters* 30 (1979), pp. 682–685.

[14] V. A. Rubakov, M. V. Sazhin, and A. V. Veryaskin. "Graviton creation in the inflationary universe and the grand unification scale". In: *Physics Letters B* 115 (1982), pp. 189–192. DOI: 10.1016/0370-2693(82)90641-4.

[15] L. F. Abbott and Mark B. Wise. "Constraints on generalized inflationary cosmologies". In: *Physics Letters B* 135 (1984), pp. 279–282. DOI: 10.1016/0370-2693(84)90637-0.

[16] Giovanni Montani et al. *Primordial Cosmology*. Singapore: World Scientific, 2011. ISBN: 978-981-4271-00-4.

[17] H. V. Ragavendra, L. Sriramkumar, and Joseph Silk. "Inflationary perturbation spectra at next-to-leading order". In: *JCAP* 02 (2023), p. 029. DOI: 10.1088/1475-7516/2023/02/029. arXiv: 2205.12608 [astro-ph.CO].

[18] Ewan D. Stewart and David H. Lyth. "A more accurate analytic calculation of the spectrum of cosmological perturbations produced during inflation". In: *Physics Letters B* 302 (1993), pp. 171–175. DOI: 10.1016/0370-2693(93)90379-V.

[19] Steven Weinberg. "Damping of tensor modes in cosmology". In: *Physical Review D* 69 (2004), p. 023503. DOI: 10.1103/PhysRevD.69.023503. arXiv: astro-ph/0306304.

[20] Yuki Watanabe and Eiichiro Komatsu. "Improved calculation of the primordial gravitational wave spectrum in the standard model". In: *Physical Review D* 73 (2006), p. 123515. DOI: 10.1103/PhysRevD.73.123515. arXiv: astro-ph/0604176.

[21] NANOGrav Collaboration, A Afzal, et al. "The NANOGrav 15-year Data Set: Search for Signals from New Physics". In: *The Astrophysical Journal Letters* 951 (2023), p. L11. DOI: 10.3847/2041-8213/acdc91.

[22] Mohamed M. Anber and Lorenzo Sorbo. "Naturally inflating on steep potentials through electromagnetic dissipation". In: *Physical Review D* 81 (2010), p. 043534. DOI: 10.1103/PhysRevD.81.043534. arXiv: 0908.4089.

[23] Neil Barnaby, Marco Peloso, and Lorenzo Sorbo. "Observable non-Gaussianity from gauge field production in slow-roll inflation, and a challenging connection with magnetogenesis". In: *Physical Review D* 85 (2012), p. 123523. DOI: 10.1103/PhysRevD.85.123523. arXiv: 1202.1469.

[24] Guillem Domènech. "Scalar-induced gravitational waves review". In: *Living Reviews in Relativity* 24 (2021), p. 7. DOI: 10.1007/s41114-021-00030-3. arXiv: 2109.01398.

[25] Kazunori Kohri and Takahiro Terada. "Semianalytic calculation of the gravitational wave spectrum nonlinearly induced from primordial curvature perturbations". In: *Physical Review D* 97 (2018), p. 123532. DOI: 10.1103/PhysRevD.97.123532. arXiv: 1804.08577.

[26] EPTA Collaboration, J Antoniadis, et al. "The second data release from the European Pulsar Timing Array III. Search for gravitational wave signals". In: *Astronomy & Astrophysics* 678 (2023), A50. DOI: 10.1051/0004-6361/202347932.

[27] Chiara Caprini et al. “Science with the space-based interferometer eLISA. II: Gravitational waves from cosmological phase transitions”. In: *JCAP* 04 (2016), p. 001. DOI: 10.1088/1475-7516/2016/04/001. arXiv: 1512.06239.

[28] Chiara Caprini et al. “Detecting gravitational waves from cosmological phase transitions with LISA: an update”. In: *JCAP* 03 (2020), p. 024. DOI: 10.1088/1475-7516/2020/03/024. arXiv: 1910.13125.

[29] Pierre Auclair et al. “Probing the gravitational wave background from cosmic strings with LISA”. In: *Living Reviews in Relativity* 23 (2020), p. 3. DOI: 10.1007/s41114-020-00030-4. arXiv: 1909.00819.

[30] EPTA Collaboration, J Antoniadis, et al. “The second data release from the European Pulsar Timing Array IV. Implications for new physics”. In: *Astronomy & Astrophysics* 685 (2024), A50. DOI: 10.1051/0004-6361/202346844.

[31] Cosimo Bambi, Stavros Katsanevas, and Kostas D. Kokkotas, eds. *Handbook of Gravitational Wave Astronomy*. Springer Nature Singapore, 2022. ISBN: 978-981-16-4306-4. DOI: 10.1007/978-981-16-4306-4.

[32] Pierre Auclair et al. “Cosmology with the Laser Interferometer Space Antenna”. In: *Living Rev. Rel.* 26.1 (2023), p. 5. DOI: 10.48550/arXiv.2204.05434. arXiv: 2204.05434 [astro-ph.CO].

[33] Planck Collaboration. “Planck 2018 results. VI. Cosmological parameters”. In: *Astronomy and Astrophysics* 641 (2020), A6. DOI: 10.1051/0004-6361/201833910. arXiv: 1807.06209.

[34] Marc Kamionkowski, Arthur Kosowsky, and Albert Stebbins. “Statistics of cosmic microwave background polarization”. In: *Phys. Rev. D* 55 (1997), pp. 7368–7388. DOI: 10.1103/PhysRevD.55.7368. arXiv: astro-ph/9611125.

[35] Deng Wang. “Primordial Gravitational Waves 2024”. In: (2024). arXiv: 2405.02103 [astro-ph.CO].

[36] NANOGrav Collaboration, G Agazie, et al. “The NANOGrav 15-year Data Set: Evidence for a Gravitational-Wave Background”. In: *The Astrophysical Journal Letters* 951 (2023), p. L8. DOI: 10.3847/2041-8213/acdac6.

[37] Ronald W. Hellings and George S. Downs. “Upper limits on the isotropic gravitational radiation background from pulsar timing analysis”. In: *The Astrophysical Journal* 265 (1983), pp. L39–L42. DOI: 10.1086/183954.

[38] Alberto Sesana and Daniel G Figueroa. “Nanohertz gravitational waves”. In: *Annual Review of Nuclear and Particle Science)* (2024). DOI: 10.48550/arXiv.2512.18822. arXiv: 2512.18822.

[39] Andrew H. Jaffe and Donald C. Backer. “Gravitational waves probe the coalescence rate of massive black hole binaries”. In: *The Astrophysical Journal* 583.2 (2003), pp. 616–631. DOI: 10.1086/345443.

[40] John Ellis et al. “What is the source of the PTA GW signal?” In: *arXiv preprint arXiv:2308.08546* (2023). DOI: 10.48550/arXiv.2308.08546. arXiv: 2308.08546 [astro-ph.CO].

[41] Daniele Bertacca et al. “Inflation without an Inflaton”. In: *Physical Review D* (2023).

[42] Alexander Vilenkin. “Creation of universes from nothing”. In: *Physics Letters B* 117.1-2 (1982), pp. 25–28. DOI: 10.1016/0370-2693(82)90530-5.

[43] Joseph D Romano and Neil J Cornish. “Detection methods for stochastic gravitational-wave backgrounds: a unified approach”. In: *Living Reviews in Relativity* 20.1 (2017), p. 2. DOI: 10.1007/s41114-017-0004-1.

[44] BICEP/Keck Collaboration. “Improved Constraints on Primordial Gravitational Waves using BICEP/Keck Data”. In: *Physical Review Letters* (2023). arXiv: 2210.17154.

[45] Travis Robson, Neil J. Cornish, and Chang Liu. “The construction and use of LISA sensitivity curves”. In: *Classical and Quantum Gravity* 36.10 (2019), p. 105011. DOI: 10.1088/1361-6382/ab1101. arXiv: 1803.01944.